High Order One-Step AMR and ALE Methods for Hyperbolic PDE

Michael Dumbser

Collaborators:

Prof. A. Hidalgo, Prof. C. Parés, Prof. M. Castro
Dr. O. Zanotti, Ing. W. Boscheri

European Research Council

Oporto, Portugal, 28/04/2014

Starting Point: Very General Form of the Governing PDE

We want to construct numerical schemes for very general hyperbolic-parabolic time-dependent partial differential equations in multiple space dimensions of the following general form:

$$\frac{\partial Q}{\partial t} + \nabla \cdot F(Q, \nabla Q) + B(Q) \cdot \nabla Q = S(Q) \qquad \text{(PDE)}$$

The nonlinear flux depends on the gradient of *Q*, to take into account also **parabolic terms**, such as **viscous effects**.
The third term is a **non-conservative** term that is important in many multi-fluid and multi-phase models.
The source term on the right hand side may also be **stiff**.

Many of the mathematical models relevant for physics and engineering can be cast in the form of eqn. (PDE).

Basic Concept of $P_N P_M$ Schemes in 1D

First-order Godunov-type finite volume schemes for (PDE):

- Data *u:* **piecewise constant** cell averages.
- Interface fluxes: computed using the **same** data *u*.

$$\frac{d}{dt}\int_{x_{i-\frac{1}{2}}}^{x_{i+\frac{1}{2}}} u\,dx = -\left(f_{i+\frac{1}{2}}(u^-_{i+\frac{1}{2}}, u^+_{i+\frac{1}{2}}) - f_{i-\frac{1}{2}}(u^-_{i-\frac{1}{2}}, u^+_{i-\frac{1}{2}}) \right) \qquad u \in P_0$$

Higher-order extension of Godunov-type finite volume schemes for (PDE):

- Data *u:* **piecewise constant** cell averages;
- Interface fluxes: computed using higher order piecewise polynomials *w* of degree *M*, computed from *u* using a **reconstruction** operator.

$$\frac{d}{dt}\int_{x_{i+\frac{1}{2}}}^{x_{i-\frac{1}{2}}} u\,dx = -\left(f_{i+\frac{1}{2}}\left(\boxed{w^-_{i+\frac{1}{2}}, w^+_{i+\frac{1}{2}}}\right) - f_{i-\frac{1}{2}}\left(\boxed{w^-_{i-\frac{1}{2}}, w^+_{i-\frac{1}{2}}}\right) \right) \qquad w \in P_M$$

Basic Concept of $P_N P_M$ Schemes in 1D

High-order Discontinuous Galerkin finite element schemes for (PDE):

- Data *u:* **piecewise polynomials** of degree *N*;
- Interface fluxes: computed using the same higher order piecewise polynomials *u* of degree *N*.

$$\frac{d}{dt}\int_{x_{i-\frac{1}{2}}}^{x_{i+\frac{1}{2}}} \Phi_k u\,dx = -\left(\Phi_k(x^-_{i+\frac{1}{2}}) f_{i+\frac{1}{2}}(u^-_{i+\frac{1}{2}}, u^+_{i+\frac{1}{2}}) - \Phi_k(x^+_{i-\frac{1}{2}}) f_{i-\frac{1}{2}}(u^-_{i-\frac{1}{2}}, u^+_{i-\frac{1}{2}})\right) + \int_{x_{i-\frac{1}{2}}}^{x_{i+\frac{1}{2}}} \frac{\partial}{\partial x}\Phi_k f(u)\,dx$$

$$u_h,\ \Phi_k \in P_N$$

High-order $P_N P_M$ schemes for (PDE):

- Data *u:* **piecewise polynomials** of degree *N*;
- Interface fluxes: computed using higher order piecewise polynomials *w* of degree *M* ≥ *N*. *w* is computed from *u* using **reconstruction**.

$$\frac{d}{dt}\int_{x_{i-\frac{1}{2}}}^{x_{i+\frac{1}{2}}} \Phi_k u\,dx = -\left(\Phi_k(x^-_{i+\frac{1}{2}}) f_{i+\frac{1}{2}}\boxed{(w^-_{i+\frac{1}{2}}, w^+_{i+\frac{1}{2}})} - \Phi_k(x^+_{i-\frac{1}{2}}) f_{i-\frac{1}{2}}\boxed{(w^-_{i-\frac{1}{2}}, w^+_{i-\frac{1}{2}})}\right) + \int_{x_{i-\frac{1}{2}}}^{x_{i+\frac{1}{2}}} \frac{\partial}{\partial x}\Phi_k f\boxed{(w)}\,dx$$

$$u_h,\ \Phi_k \in P_N; \quad w_h \in P_M$$

General $P_N P_M$ Schemes on Unstructured Meshes

Throughout this presentation the following three operators will be used:

$$\langle f, g \rangle_{T_i} = \int_{t^n}^{t^{n+1}} \int_{T_i} \left(f(\vec{x}, t) \cdot g(\vec{x}, t) \right) dV\, dt, \qquad \text{(OP1)}$$

$$[f, g]_{T_i}^{t} = \int_{T_i} \left(f(\vec{x}, t) \cdot g(\vec{x}, t) \right) dV, \qquad \text{(OP2)}$$

$$\{f, g\}_{\partial T_i} = \int_{t^n}^{t^{n+1}} \int_{\partial T_i} \left(f(\vec{x}, t) \cdot g(\vec{x}, t) \right) dS\, dt, \qquad \text{(OP3)}$$

General $P_N P_M$ Schemes on Unstructured Meshes

1. Reconstruction of piecewise polynomials *w* of degree *M* from piecewise polynomials *u* of degree *N* using *L2*-projection on a stencil S_i :

$$u_h(\vec{x},t^n) = \sum_l \Phi_l(\vec{x})\hat{u}_l^n \qquad w_h(\vec{x},t^n) = \sum_l \Psi_l(\vec{x})\hat{w}_l^n$$

Stencil definition: $\mathscr{S}_i = \bigcup_{k=1}^{n_e} T_{j(k)}$

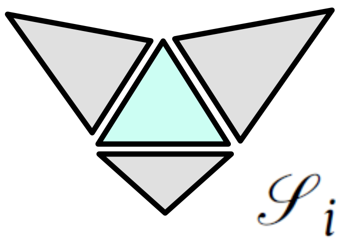

Reconstruction equations (*L2*-projection):

$$[\Phi_k, w_h]_{T_j}^{t^n} = [\Phi_k, u_h]_{T_j}^{t^n} \quad \forall T_j \in \mathscr{S}_i.$$

The reconstruction equations are solved using constrained LSQ. Monotonicity is enforced using a nonlinear WENO reconstruction.

General $P_N P_M$ Schemes on Unstructured Meshes

1. Reconstruction of piecewise polynomials *w* of degree *M* from piecewise polynomials *u* of degree *N* using *L2*-projection on a stencil S_i :

$\mathcal{O}(1)$	P_0P_0			
$\mathcal{O}(2)$	P_0P_1	P_1P_1		
$\mathcal{O}(3)$	P_0P_2	P_1P_2	P_2P_2	
$\mathcal{O}(4)$	P_0P_3	P_1P_3	P_2P_3	P_3P_3
$\vdots$				
$\mathcal{O}(M+1)$	P_0P_M $\cdots$	P_NP_M $\cdots$	P_MP_M	
	FV	new class	DG	

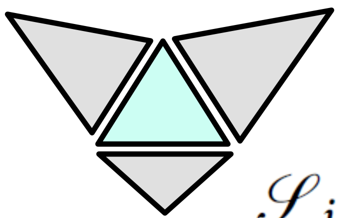

$\mathcal{S}_i$

General $P_N P_M$ Schemes on Unstructured Meshes

2. Local predictor that computes a solution *in the small* of the local Cauchy-Problem for (PDE) with initial data w_h. This allows the construction of **high order one-step** schemes in time.

   - Cauchy-Kovalewski procedure, based on Taylor series and successive differentiation of the governing PDE. Disadvantages: not able to treat stiff sources, not applicable to general PDE.

   - Element-local discontinuous space-time Galerkin predictor. Applicable to general PDE with **stiff** source terms.

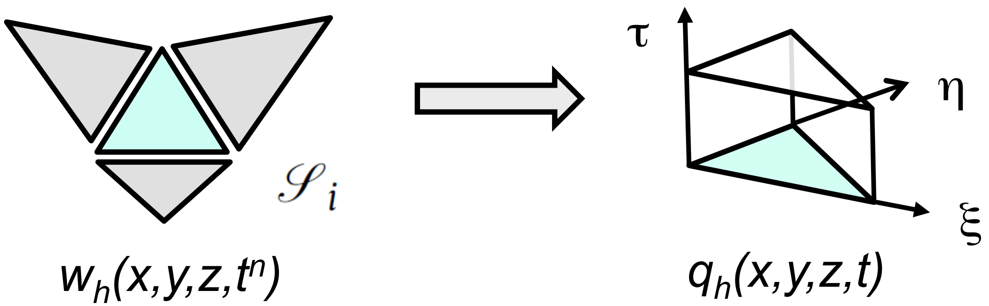

Local Space-Time DG Predictor Method

PDE transformed to the space-time reference element

$$\frac{\partial}{\partial \tau} Q + \nabla_\xi \cdot F^* \left(Q, \nabla Q\right) = S^* - B^*(Q) \cdot \nabla Q := P^*(Q, \nabla Q)$$

Multiplication with a piecewise polynomial space-time test function of degree *M* and integration in space and time yields

$$\left\langle \theta_k, \frac{\partial}{\partial \tau} q_h \right\rangle + \left\langle \theta_k, \nabla_\xi \cdot F^* \left(q_h, \nabla q_h\right)\right\rangle = \left\langle \theta_k, P^* \left(q_h, \nabla q_h\right)\right\rangle$$

Element-local space-time ansatz

$$q_h = q_h(\vec{\xi}, \tau) = \sum_l \theta_l(\vec{\xi}, \tau)\hat{q}_l := \theta_l \hat{q}_l \qquad \mathcal{F}_h^* = \mathcal{F}_h^*(\vec{\xi}, \tau) = \sum_l \theta_l(\vec{\xi}, \tau)\hat{\mathcal{F}}_l := \theta_l \hat{\mathcal{F}}_l,$$

$$\nabla_\xi q_h = \nabla_\xi q_h(\vec{\xi}, \tau) = \sum_l \theta_l(\vec{\xi}, \tau)\hat{q}_l' := \theta_l \hat{q}_l', \qquad \mathcal{P}_h^* = \mathcal{P}_h^*(\vec{\xi}, \tau) = \sum_l \theta_l(\vec{\xi}, \tau)\hat{P}_l := \theta_l \hat{P}_l,$$

Integration by parts **in time** only

$$\left[\theta_k, q_h\right]^1 - \left[\theta_k w_h\right]^0 - \left\langle \frac{\partial}{\partial \tau}\theta_k, q_h \right\rangle + \left\langle \theta_k, \nabla_\xi \cdot F^* \left(q_h, \nabla q_h\right)\right\rangle = \left\langle \theta_k, P^*(q_h, \nabla q_h)\right\rangle .$$

Local Space-Time DG Predictor Method

Inserting the polynomial ansatz yields

$$\left([\theta_k, \theta_l]^1 - \left\langle \frac{\partial}{\partial \tau}\theta_k, \theta_l \right\rangle \right) \hat{q}_l^{i+1} = [\theta_k, \psi_m]^0 \hat{w}_m^n + \langle \theta_k, \theta_l \rangle \; \hat{P}_l^i - \langle \theta_k, \nabla_\xi \theta_l \rangle \cdot \hat{\mathcal{F}}_l^i$$

Or, in more compact matrix-vector notation, we get the following **element-local** equation system

$$K_1 \hat{q}_l = F_0 \hat{w}_m^n + M \hat{P}_l - K_\xi \cdot \hat{\mathcal{F}}_l$$

For its solution, we use the following fixed-point iteration scheme:

$$K_1 \hat{q}_l^{i+1} = F_0 \hat{w}_m^n + M \hat{P}_l^i - K_\xi \cdot \hat{\mathcal{F}}_l^i \qquad \text{(FP)}$$

In the **stiff** case, the source term is taken **locally implicitly** in (FP).

General $P_N P_M$ Schemes on Unstructured Meshes

3. **Explicit** global corrector scheme

Multiply eqn. (PDE) with spatial test functions ϕ_k (piecewise polynomials of degree N) and integrate in space and time:

$$\left\langle \Phi_k, \frac{\partial}{\partial t} Q \right\rangle_{T_i} + \langle \Phi_k, \nabla \cdot F(Q, \nabla Q) + B(Q) \cdot \nabla Q \rangle_{T_i} = \langle \Phi_k, S(Q) \rangle_{T_i}$$

Integration by parts in time yields then the fully-discrete $P_N P_M$ scheme

$$\left[\Phi_k, u_h^{n+1}\right]_{T_i}^{t^{n+1}} - \left[\Phi_k, u_h^{n}\right]_{T_i}^{t^{n}} + \langle \Phi_k, \nabla F(q_h, \nabla q_h) + B(q_h) \cdot \nabla q_h \rangle_{T_i \setminus \partial T_i}$$
$$+ \left\{ \Phi_k, \mathcal{D}^-_{i+\frac{1}{2}}(q_h^-, \nabla q_h^-, q_h^+, \nabla q_h^+) \cdot \vec{n} \right\}_{\partial T_i} = \langle \Phi_k, S(q_h) \rangle_{T_i} \,,$$

with a path-conservative jump term [Toumi 1992, Parés 2006, Castro et al. 2006], consistent with the theory of [Dal Maso, Le Floch and Murat, 1995].
If the PDE is conservative (*B(Q)*=0), then the method reduces to a classical fully conservative scheme.

Summary of the Algorithm

(1) Use the $P_N P_M$ reconstruction operator at the current time t^n to reconstruct the polynomials *w* of degree *M* from the polynomials *u* of degree *N* that are stored and evolved in each cell.

$$w_h^n = \mathcal{R}_h\left(u_h^n\right)$$

(2) Use the **local** space-time DG predictor method to obtain for each cell a space-time *predictor* polynomial of degree *M,* valid in the time interval $[t^n, t^{n+1}]$.

$$q_h = \mathcal{E}_h\left(w_h^n\right)$$

(3) Use the globally explicit one-step corrector scheme to evolve the piecewise polynomial data *u* of degree *N* from time t^n to time t^{n+1}.

$$u_h^{n+1} = u_h^n + \mathcal{P}_{\mathcal{N}}^{\mathcal{M}}\left(q_h, \nabla q_h\right)$$

Special cases:

$N = 0$: classical high order finite volume scheme

$N = M$: usual DG finite element scheme

The Fully-Discrete $P_N P_M$ Scheme

Using linear von Neumann stability analysis for the linear scalar advection equation in 1D yields the following stability limits for $P_N P_M$ schemes:

$\mathrm{CFL}_{\max}$	$N=0$	$N=1$	$N=2$	$N=3$	$N=4$
$M=1$	1.00	0.33			
$M=2$	1.00	0.32	0.17		
$M=3$	1.00	0.32	0.17	0.10	
$M=4$	1.00	0.32	0.17	0.10	0.069

From these results, we conclude that it is the degree *N* of the polynomials representing the data that imposes the time step limit and not the degree *M* of the reconstruction polynomials.

$P_N P_M$ schemes have larger time steps than pure DG schemes of the same order of accuracy.

Compressible Navier-Stokes Equations

This well-known governing PDE system is defined by

Convective and viscous flux tensor

$$\underline{\underline{F}}(W,\nabla W) = \begin{pmatrix} \vec{v}^T \rho \\ \vec{v}^T \otimes \rho \vec{v} + \underline{\underline{\sigma}}(W,\nabla W) \\ \vec{v}^T(\mathbf{I}\rho E + \underline{\underline{\sigma}}(W,\nabla W)) - \kappa \nabla T, \end{pmatrix} \qquad \kappa = \frac{\mu \gamma c_v}{Pr}$$

Stress tensor of a Newtonian fluid

$$\underline{\underline{\sigma}} = \left(p + \frac{2}{3}\mu \nabla \cdot \vec{v}\right)\mathbf{I} - \mu\left(\nabla \vec{v} + \nabla \vec{v}^T\right)$$

Ideal gas EOS

$$p = (\gamma - 1)\left(\rho E - \frac{1}{2}\rho \vec{v}^{\,2}\right)$$

Sutherland‘s law

$$\mu(T) = \mu_0 \left(\frac{T}{T_0}\right)^\beta \frac{T_0 + s}{T + s}$$

Convergence Study: Compressible Navier-Stokes Equations

Numerical convergence study of P_NP_M schemes from third to sixth order of accuracy in space and time applied to the 2D compressible Navier–Stokes equations. Error norms refer to variable u and the CPU times for each method (printed in bold letters) are shown for the computation on the finest mesh.

N_G	L^2	$\mathcal{O}_{L^2}$	L^2	$\mathcal{O}_{L^2}$	L^2	$\mathcal{O}_{L^2}$	L^2	$\mathcal{O}_{L^2}$	L^2	$\mathcal{O}_{L^2}$	L^2	$\mathcal{O}_{L^2}$
$\mathcal{O}3$	P_0P_2		P_1P_2		P_2P_2							
24/16	5.11E−03		2.12E−03		1.35E−03							
32/24	2.31E−03	2.8	6.19E−04	3.0	3.24E−04	3.5						
64/32	3.35E−04	2.8	2.65E−04	3.0	1.35E−04	3.0						
128/64	5.70E−05	2.6	3.31E−05	3.0	2.24E−05	2.6						
CPU	**3011 s**		**1355 s**		**3621 s**							
$\mathcal{O}4$	P_0P_3		P_1P_3		P_2P_3		P_3P_3					
24/16	1.10E−03		1.26E−03		3.04E−04		1.67E−04					
32/24	3.61E−04	3.9	2.59E−04	3.9	5.93E−05	4.0	3.20E−05	4.1				
64/32	2.77E−05	3.7	8.76E−05	3.8	1.89E−05	4.0	1.04E−05	3.9				
128/64	2.49E−06	3.5	5.24E−06	4.1	1.09E−06	4.1	6.62E−07	4.0				
CPU	**5279 s**		**2303 s**		**6224 s**		**12,910 s**					
$\mathcal{O}5$	P_0P_4		P_1P_4		P_2P_4		P_3P_4		P_4P_4			
24/8	6.13E−04		5.74E−03		2.14E−03		8.21E−04		5.17E−04			
32/16	1.58E−04	4.7	1.93E−04	4.9	7.88E−05	4.8	2.74E−05	4.9	1.34E−05	5.3		
64/24	5.25E−06	4.9	2.67E−05	4.9	1.19E−05	4.7	3.76E−06	4.9	1.38E−06	5.6		
128/32	2.14E−07	4.6	7.07E−06	4.6	2.84E−06	5.0	8.90E−07	5.0	2.88E−07	5.5		
CPU	**12,532 s**		**293 s**		**751 s**		**1842 s**		**2965 s**			
$\mathcal{O}6$	P_0P_5		P_1P_5		P_2P_5		P_3P_5		P_4P_5		P_5P_5	
24/4	1.45E−04		1.07E−02		1.97E−02		1.07E−02		4.26E−03		3.20E−03	
32/8	2.89E−05	5.6	3.05E−04	5.1	7.55E−04	4.7	3.05E−04	5.1	1.10E−04	5.3	8.19E−05	5.3
64/16	5.12E−07	5.8	6.43E−06	5.6	1.76E−05	5.4	6.43E−06	5.6	1.58E−06	6.1	9.03E−07	6.5
128/24	1.21E−08	5.4	5.79E−07	5.9	1.68E−06	5.8	5.79E−07	5.9	1.26E−07	6.2	6.31E−08	6.6
CPU	**16,267 s**		**215 s**		**558 s**		**1057 s**		**1719 s**		**2498 s**	

Compressible Mixing Layer 2D

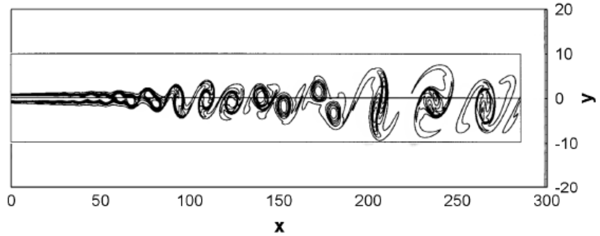

Reference solution of Colonius et al. [JFM, 1997]
$M_0 = 0.25$, $M_1 = 0.5$, $Re_\delta = 500$, $Pr = 1$

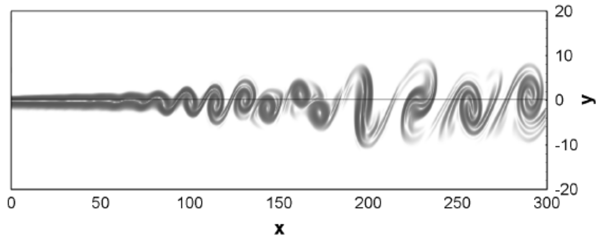

Sixth order P_0P_5 finite volume scheme.
Wallclock time: 14.75 h

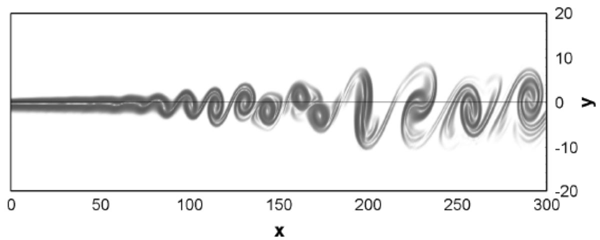

Sixth order P_3P_5 scheme.
Wallclock time: 5 h

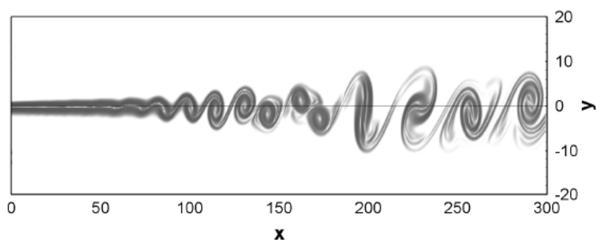

Sixth order P_5P_5 discontinuous Galerkin scheme.
Wallclock time: 8 h

Viscous & Resistive MHD Equations

Conserved variables $$W = \left(\rho, \rho\vec{v}^T, \rho E, \vec{B}^T, \psi\right)^T$$

Convective and viscous flux tensor

$$\underline{\underline{F}}(W, \nabla W) = \begin{pmatrix} \rho\vec{v}^T \\ \rho\vec{v}\vec{v}^T + \underline{\underline{\sigma}}(W, \nabla W) \\ \vec{v}^T\left(\mathbf{I}\rho E + \underline{\underline{\sigma}}(W, \nabla W)\right) - \kappa\nabla T - \frac{\eta}{4\pi}\vec{B}^T\left(\nabla\vec{B} - \nabla\vec{B}^T\right) \\ \vec{B}\vec{v}^T - \vec{v}\vec{B}^T + \psi\mathbf{I} - \eta\left(\nabla\vec{B} - \nabla\vec{B}^T\right) \\ c_0^2\vec{B}^T \end{pmatrix}$$

Stress tensor of a Newtonian fluid

$$\underline{\underline{\sigma}} = \left(p + \frac{1}{8\pi}\vec{B}^2 + \frac{2}{3}\mu\nabla\cdot\vec{v}\right)\mathbf{I} - \frac{1}{4\pi}\vec{B}\vec{B}^T - \mu\left(\nabla\vec{v} + \nabla\vec{v}^T\right)$$

Here, the div B = 0 constraint may <u>not</u> be satisfied <u>exactly</u> on the discrete level, but the hyperbolic divergence cleaning strategy of <u>Dedner et al.</u> (2002) is used. Analogy with the method of artificial compressibility of Chorin (1967) for inc. NS. Divergence errors cannot accumulate locally.

Asymptotic limit: $\mathrm{div}\,B \to 0 \quad \text{if} \quad c_0 \to \infty$

VRMHD Code Validation: Laminar Boundary Layer

For further validation, we solve a high Reynolds number steady laminar boundary layer problem on a highly stretched unstructured triangular mesh. Reference solution computed by solving the nonlinear ODE system of [Shukhman, JFM 2002].

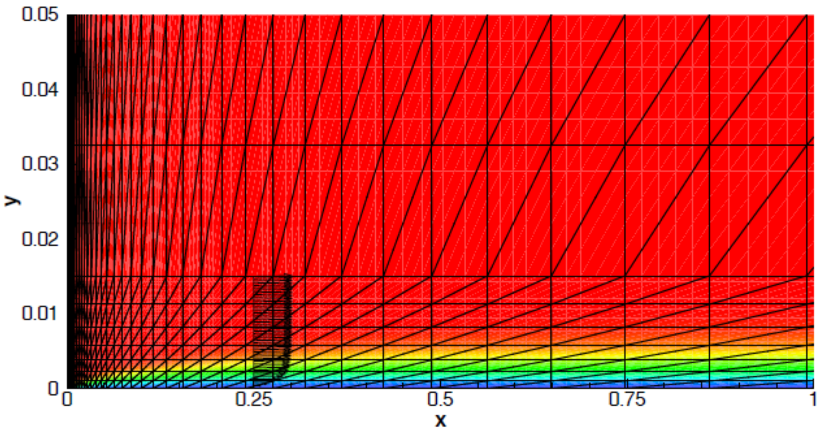

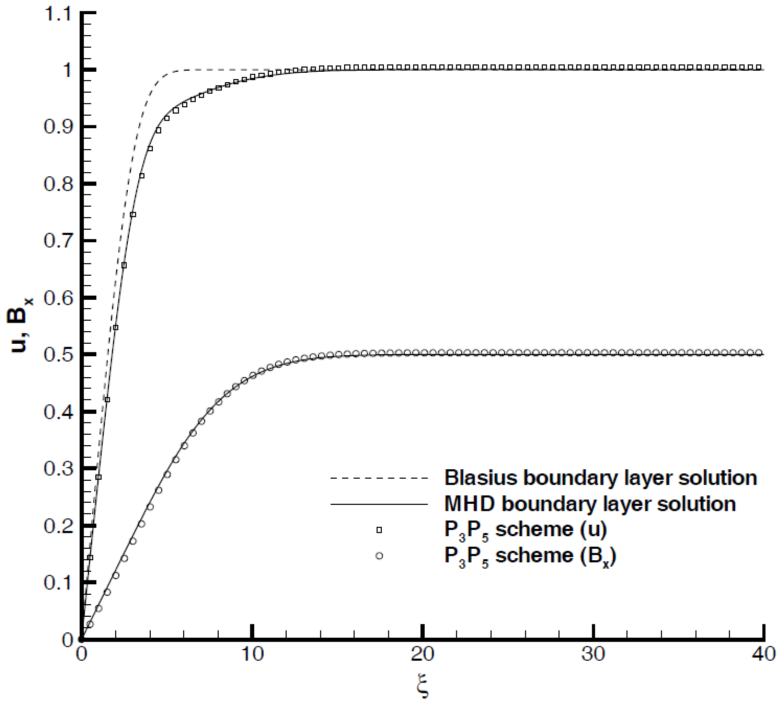

Unstructured mesh with
1430 triangular elements

$Re = 10^6$, $Pr = 1$, $Pr_m = 10^{-1}$

2D Kelvin-Helmholtz Instability

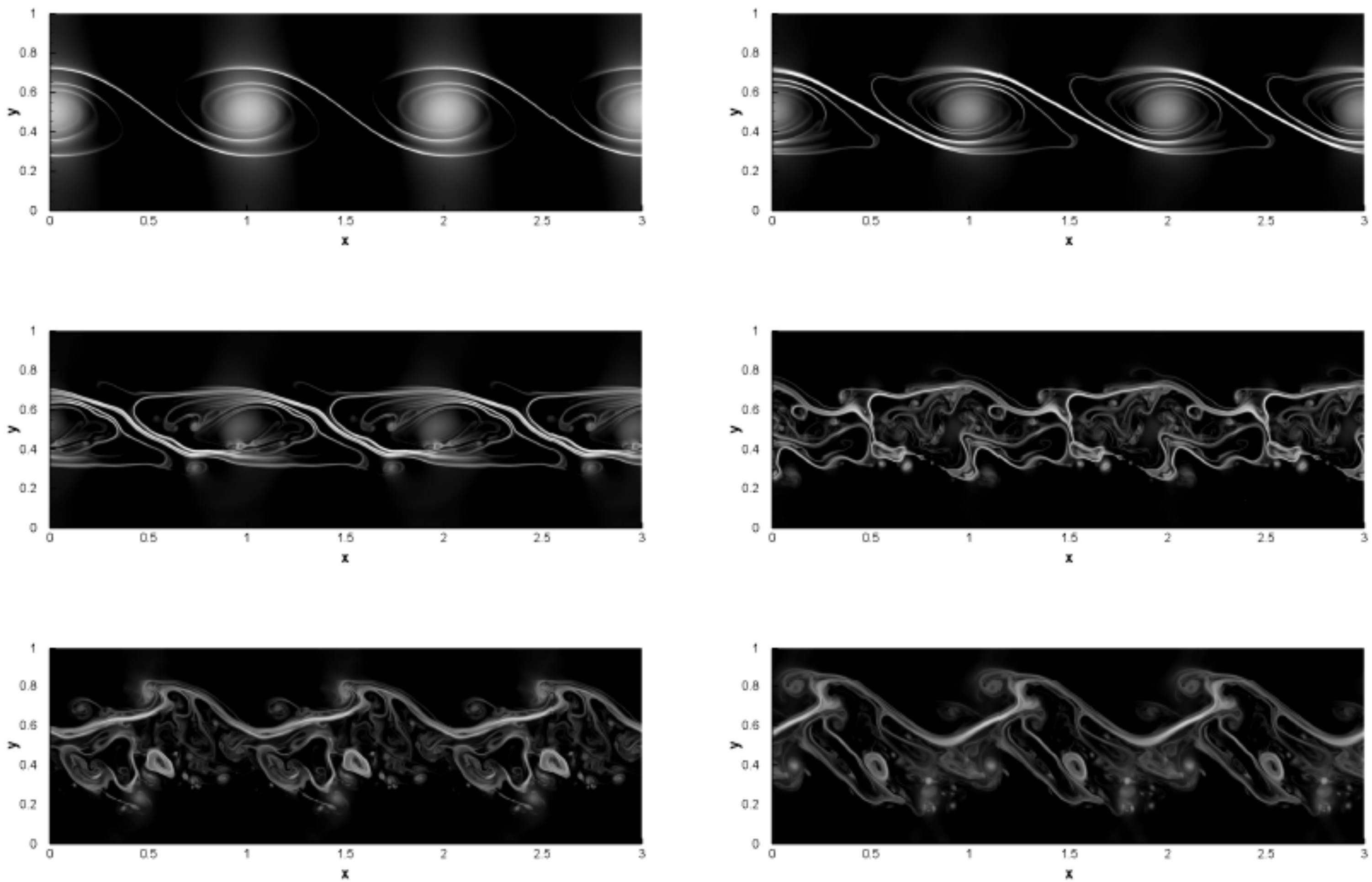

P_3P_5 on unstructured mesh with 140676 triangular elements (h=1/250)

Setup of [Jeong et al. 2000]
Re = 10^5, Pr = 1, Pr_m = 1

3D Kelvin-Helmholtz Instability

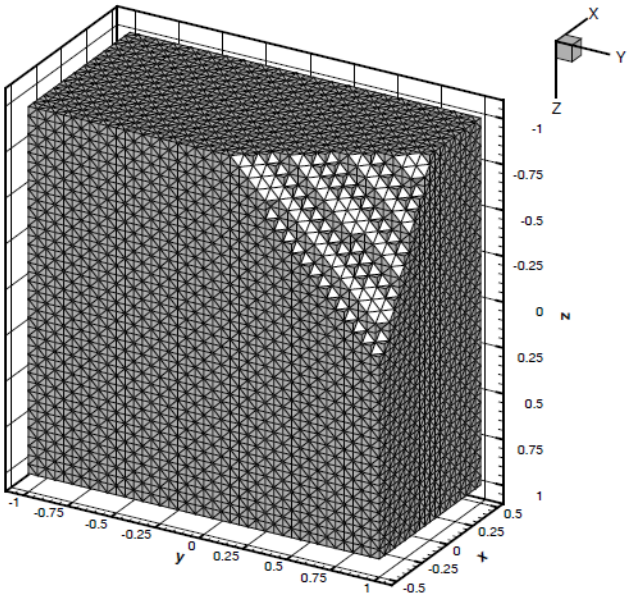

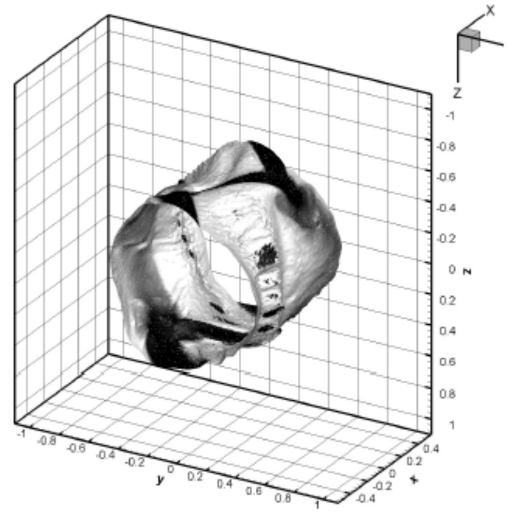

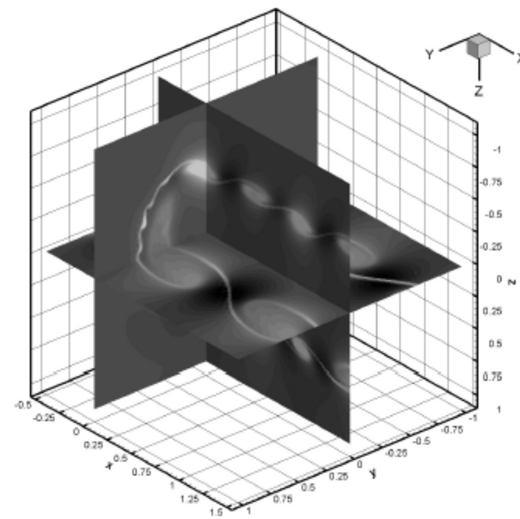

P_2P_4 on unstructured mesh with 655360 tetra elements (23e6 DOF). Setup of Keppens & Toth (1999)

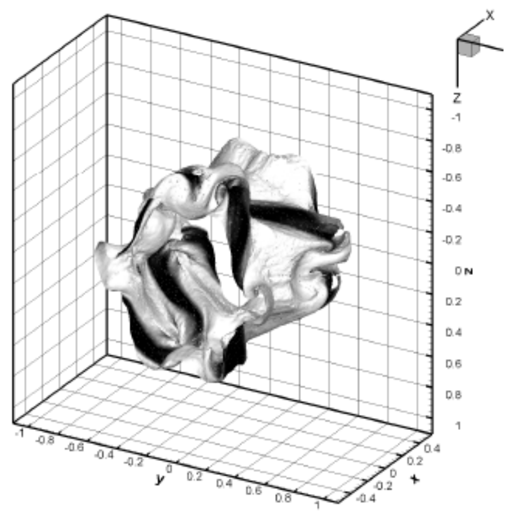

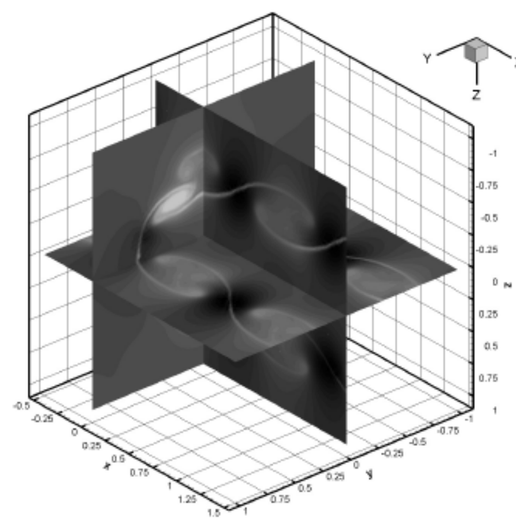

$Re = 10^4$, $Pr = 1$, $Pr_m = 1$

Convergence Study with Stiff Source Terms (RRMHD)

To verify the order of accuracy, we use the resistive **relativistic** MHD (RRMHD) equations. In the stiff case ($\sigma \to \infty$) the system tends to the **ideal** relativistic MHD (RMHD) equations, for which exact solutions are known [Del Zanna et al. 2007].

Governing PDE System

$$\partial_t D + \partial_i (D v^i) = 0,$$

$$\partial_t S_j + \partial_i Z^i_j = 0,$$

$$\partial_t \tau + \partial_i S^i = 0,$$

$$\partial_t E^i - \epsilon^{ijk} \partial_j B_k + \partial_i \Psi = -J^i,$$

$$\partial_t B^i + \epsilon^{ijk} \partial_j E_k + \partial_i \Phi = 0,$$

$$\partial_t \Psi + \partial_i E^i = \rho_c - \kappa \Psi,$$

$$\partial_t \Phi + \partial_i B^i = -\kappa \Phi,$$

$$\partial_t \rho_c + \partial_i J^i = 0,$$

Conserved quantities

$$D = \rho \Gamma,$$

$$S^i = \omega \Gamma^2 v^i + \epsilon^{ijk} E_j B_k,$$

$$\tau = \omega \Gamma^2 - p + \frac{1}{2}(E^2 + B^2),$$

Variables used in the fluxes

$$Z^i_j = \omega \Gamma^2 v^i v_j - E^i E_j - B^i B_j + \left[p + \frac{1}{2}(E^2 + B^2) \right] \delta^i_j$$

$$p = (\gamma - 1)\rho \epsilon = \gamma_1 (\omega - \rho)$$

Ohm's law (**stiff** source term)

$$\vec{J} = \rho_c \vec{v} + \boxed{\sigma \Gamma} [\vec{E} + \vec{v} \times \vec{B} - (\vec{E} \cdot \vec{v}) \vec{v}]$$

Convergence Study with Stiff Source Terms (RRMHD)

Table 1
Large amplitude Alfvén wave. Convergence study of P_NP_M schemes from third to fifth order of accuracy. $\sigma = 10^7$, apart from the P_1P_4 scheme where $\sigma = 10^8$. Errors are computed for variable B_y.

P_0P_2			P_1P_2			P_2P_2		
N_G	L^2	$\mathcal{O}_{L^2}$	N_G	L^2	$\mathcal{O}_{L^2}$	N_G	L^2	$\mathcal{O}_{L^2}$
16	1.71E−02		8	9.12E−04		8	8.97E−04	
24	5.32E−03	2.9	12	2.26E−04	3.4	12	2.92E−04	2.8
32	2.26E−03	3.0	16	9.34E−05	3.1	16	1.67E−04	1.9
64	2.79E−04	3.0	24	2.53E−05	3.2	24	4.98E−05	3.0
P_0P_3			P_1P_3			P_1P_4		
12	1.81E−03		4	7.18E−03		4	3.32E−03	
16	4.52E−04	4.8	8	3.75E−04	4.3	8	2.95E−05	6.8
24	7.35E−05	4.5	12	7.91E−05	3.8	12	4.46E−06	4.7
32	1.98E−05	4.6	16	2.82E−05	3.6	16	1.07E−06	5.0

Table 2
Large amplitude Alfvén wave. Verification of the order of accuracy for a variable affected by the stiff source term. We use the quantity E_y and some selected P_NP_M schemes.

P_0P_2			P_0P_3			P_1P_4		
N_G	L^2	$\mathcal{O}_{L^2}$	N_G	L^2	$\mathcal{O}_{L^2}$	N_G	L^2	$\mathcal{O}_{L^2}$
16	7.66E−03		12	6.09E−04		4	9.43E−04	
24	1.90E−03	3.4	16	2.11E−04	3.7	8	1.22E−05	6.3
32	7.75E−04	3.1	24	4.02E−05	4.1	12	2.06E−06	4.4
64	9.56E−05	3.0	32	1.14E−05	4.4	16	5.18E−07	4.8

Asymptotic Preserving Property: 2D Blast Wave

E_z

p

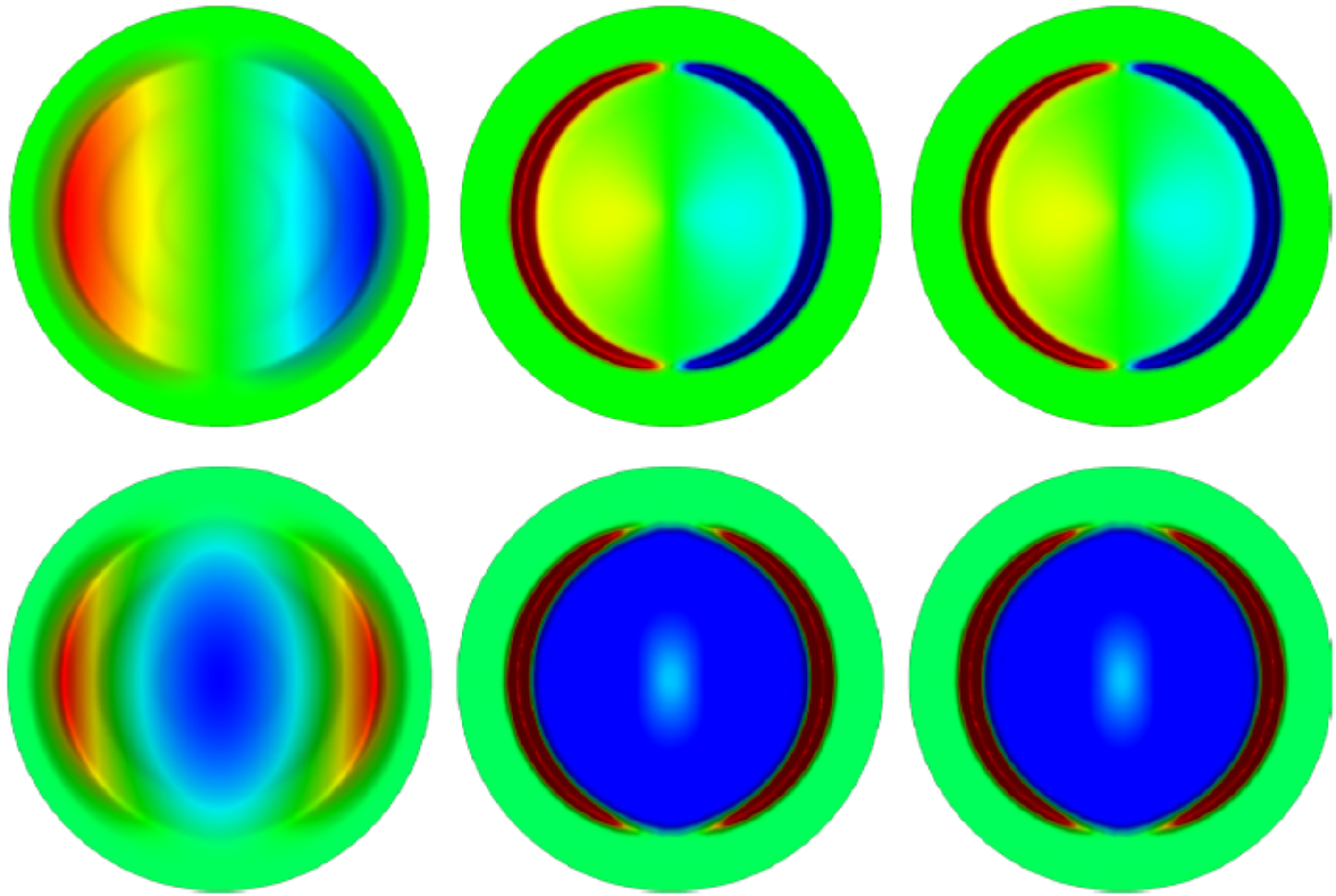

$\sigma = 1.0$ | $\sigma = 10^5$ | ideal RMHD

Convergence of RRMHD to ideal RMHD for large values of σ. P_0P_2 scheme.

Can we extend these schemes also to

i) space-time adaptive mesh refinement (AMR)
ii) and to moving unstructured meshes?

High-Order One-Step AMR

An integral finite volume formulation of (PDE) reads

$$
\begin{aligned}
\bar{\mathbf{u}}_{ijk}^{n+1} = \bar{\mathbf{u}}_{ijk}^{n} & - \frac{\Delta t}{\Delta x_i}\left[\left(\mathbf{f}_{i+\frac{1}{2},j,k} - \mathbf{f}_{i-\frac{1}{2},j,k}\right) + \frac{1}{2}\left(D^x_{i+\frac{1}{2},j,k} + D^x_{i-\frac{1}{2},j,k}\right)\right] \\
& - \frac{\Delta t}{\Delta y_j}\left[\left(\mathbf{g}_{i,j+\frac{1}{2},k} - \mathbf{g}_{i,j-\frac{1}{2},k}\right) + \frac{1}{2}\left(D^y_{i,j+\frac{1}{2},k} + D^y_{i,j-\frac{1}{2},k}\right)\right] \\
& - \frac{\Delta t}{\Delta z_k}\left[\left(\mathbf{h}_{i,j,k+\frac{1}{2}} - \mathbf{h}_{i,j,k-\frac{1}{2}}\right) + \frac{1}{2}\left(D^z_{i,j,k+\frac{1}{2}} + D^z_{i,j,k-\frac{1}{2}}\right)\right] \\
& + \Delta t(\bar{\mathbf{S}}_{ijk} - \bar{\mathbf{P}}_{ijk}),
\end{aligned}
$$

with the cell average

$$
\bar{\mathbf{u}}_{ijk}^{n} = \frac{1}{\Delta x_i}\frac{1}{\Delta y_j}\frac{1}{\Delta z_k}\int_{x_{i-\frac{1}{2}}}^{x_{i+\frac{1}{2}}}\int_{y_{j-\frac{1}{2}}}^{y_{j+\frac{1}{2}}}\int_{z_{k-\frac{1}{2}}}^{z_{k+\frac{1}{2}}} \mathbf{u}(x,y,z,t^n)dz\,dy\,dx
$$

and with the fluxes, jump and source terms defined as

High-Order One-Step AMR

$$\mathbf{f}_{i+\frac{1}{2},jk} = \frac{1}{\Delta t}\frac{1}{\Delta y_j}\frac{1}{\Delta z_k}\int_{t^n}^{t^{n+1}}\int_{y_{j-\frac{1}{2}}}^{y_{j+\frac{1}{2}}}\int_{z_{k-\frac{1}{2}}}^{z_{k+\frac{1}{2}}} \tilde{\mathbf{f}}\left(\mathbf{q}_h^-(x_{i+\frac{1}{2}},y,z,t),\mathbf{q}_h^+(x_{i+\frac{1}{2}},y,z,t)\right) dz\,dy\,dt,$$

$$D^x_{i+\frac{1}{2},j,k} = \frac{1}{\Delta t}\frac{1}{\Delta y_j}\frac{1}{\Delta z_k}\int_{t^n}^{t^{n+1}}\int_{y_{j-\frac{1}{2}}}^{y_{j+\frac{1}{2}}}\int_{z_{k-\frac{1}{2}}}^{z_{k+\frac{1}{2}}} \mathcal{D}_1\left(\mathbf{q}_h^-(x_{i+\frac{1}{2}},y,z,t),\mathbf{q}_h^+(x_{i+\frac{1}{2}},y,z,t)\right) dz\,dy\,dt,$$

$$\bar{\mathbf{P}}_{ijk} = \frac{1}{\Delta t}\frac{1}{\Delta x_i}\frac{1}{\Delta y_j}\frac{1}{\Delta z_k}\int_{t^n}^{t^{n+1}}\int_{x_{i-\frac{1}{2}}}^{x_{i+\frac{1}{2}}}\int_{y_{j-\frac{1}{2}}}^{y_{j+\frac{1}{2}}}\int_{z_{k-\frac{1}{2}}}^{z_{k+\frac{1}{2}}} \mathbf{B}(\mathbf{q}_h)\cdot\nabla\mathbf{q}_h \; dz\; dy\; dx\; dt$$

$$\bar{\mathbf{S}}_{ijk} = \frac{1}{\Delta t}\frac{1}{\Delta x_i}\frac{1}{\Delta y_j}\frac{1}{\Delta z_k}\int_{t^n}^{t^{n+1}}\int_{x_{i-\frac{1}{2}}}^{x_{i+\frac{1}{2}}}\int_{y_{j-\frac{1}{2}}}^{y_{j+\frac{1}{2}}}\int_{z_{k-\frac{1}{2}}}^{z_{k+\frac{1}{2}}} \mathbf{S}\left(\mathbf{q}_h(x,y,z,t)\right) dz\,dy\,dx\,dt\,.$$

High-Order One-Step AMR

The non-conservative products are treated again using a **path-conservative approach** [Parés 2006, Castro et al. 2006]

$$\mathcal{D}_m(\mathbf{q}_h^-,\mathbf{q}_h^+) = \int_0^1 \mathbf{B}_m\left(\Psi(\mathbf{q}_h^-,\mathbf{q}_h^+,s)\right)\frac{\partial\Psi}{\partial s}ds,$$

With the straight-line segment path

$$\Psi = \Psi(\mathbf{q}_h^-,\mathbf{q}_h^+,s) = \mathbf{q}_h^- + s(\mathbf{q}_h^+ - \mathbf{q}_h^-)\,, \qquad 0 \le s \le 1.$$

one obtains the discrete jump term...

$$\mathcal{D}_m(\mathbf{q}_h^-,\mathbf{q}_h^+) = \left(\int_0^1 \mathbf{B}_m\left(\Psi(\mathbf{q}_h^-,\mathbf{q}_h^+,s)\right)ds\right)(\mathbf{q}_h^+ - \mathbf{q}_h^-)$$

as well as a very natural formulation for an Osher-type numerical flux.

$$\tilde{\mathbf{f}}\left(\mathbf{q}_h^-,\mathbf{q}_h^+\right) = \frac{1}{2}\left(\mathbf{f}(\mathbf{q}_h^+) + \mathbf{f}(\mathbf{q}_h^-)\right) + \frac{1}{2}\left(\int_0^1 |\mathbf{A}_1(\Psi)|ds\right)(\mathbf{q}_h^+ - \mathbf{q}_h^-)$$

All integrals are evaluated **numerically** using **Gauss-Legendre** quadrature.

AMR Grid and Data Structure

One refinement level & virtual cells

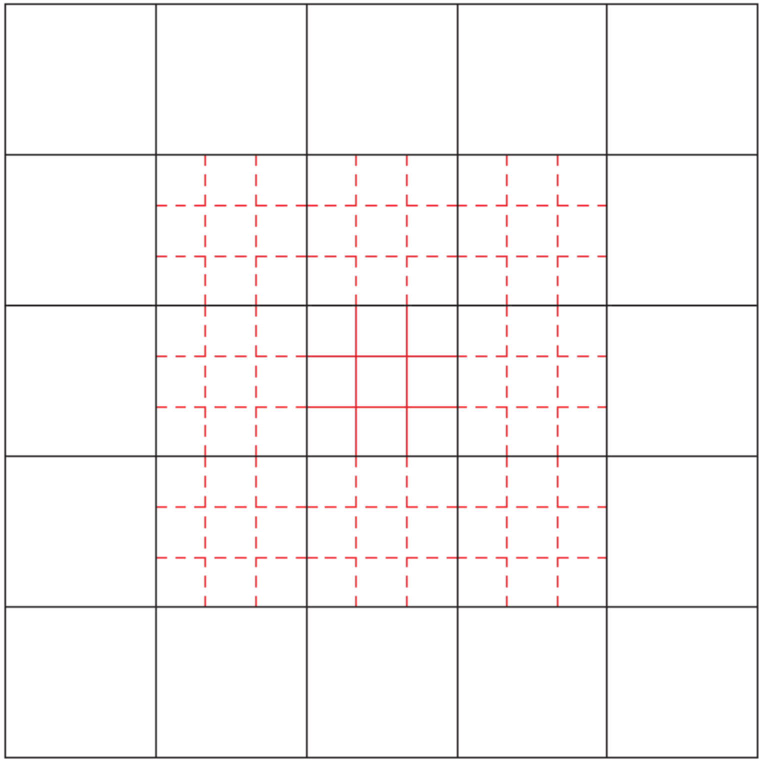

Two refinement levels & virtual cells

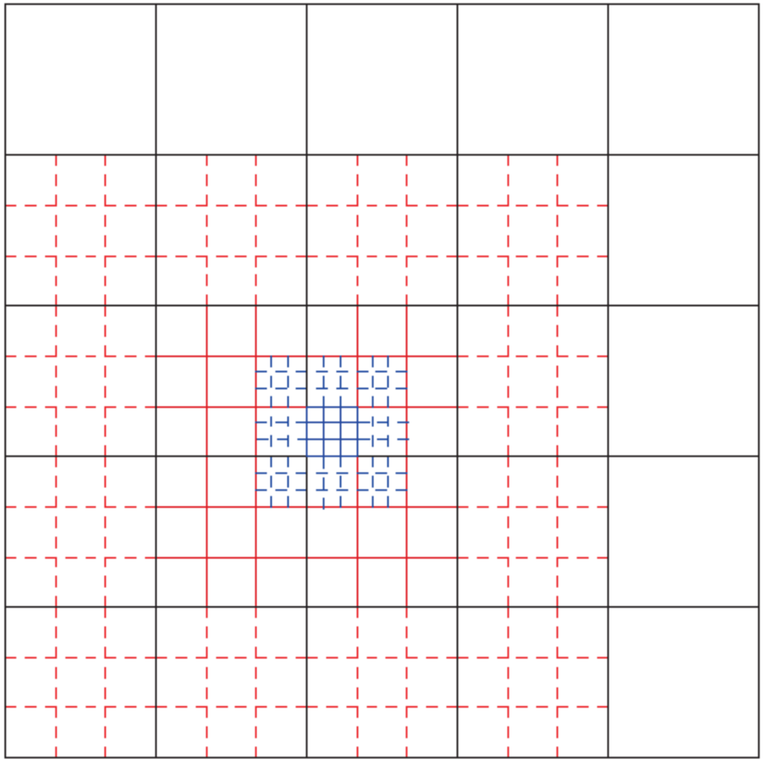

AMR Grid and Data Structure

Data are organized in a tree. There are real cells, as well as virtual coarse and fine cells, needed for the projection and averaging (prolongation and restriction) operators.

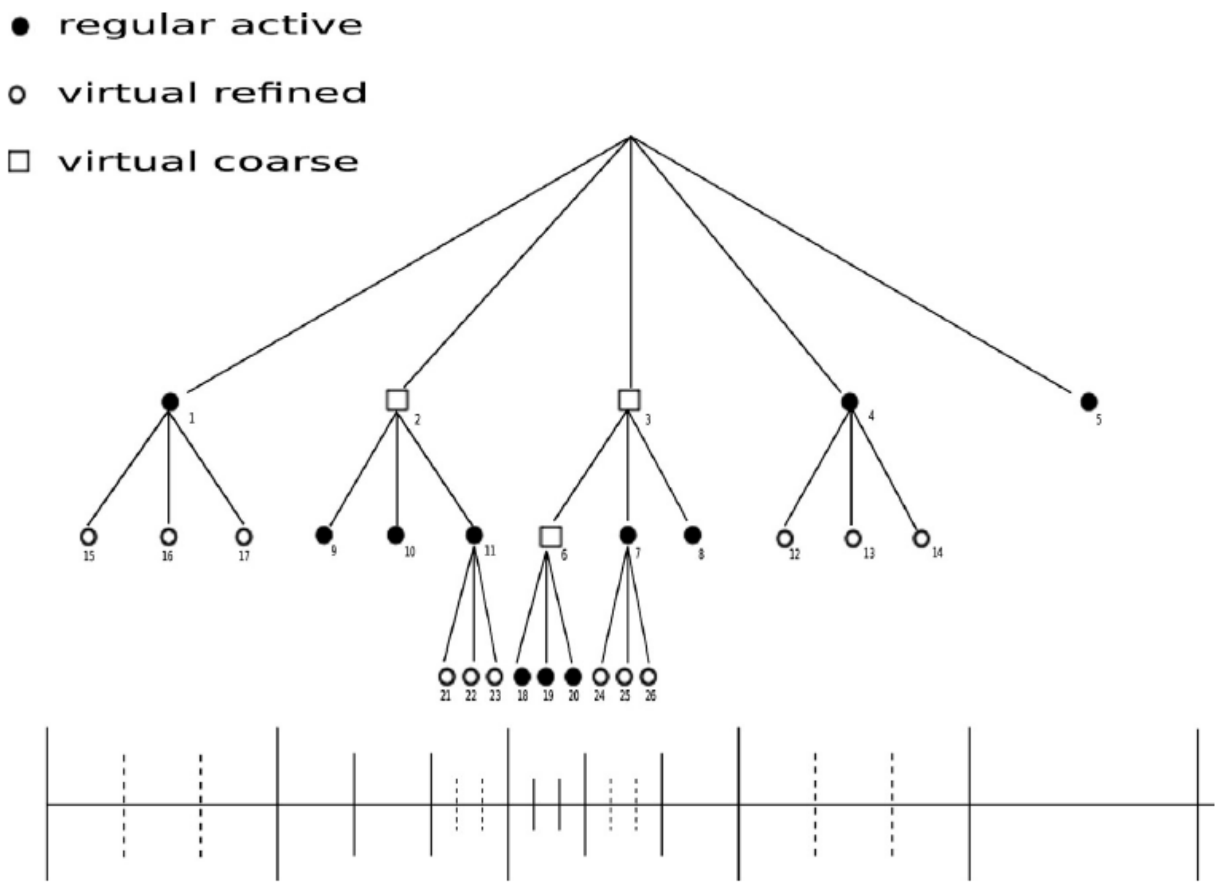

AMR with Time-Accurate Local Time Stepping (LTS)

Update criterion:

Update the highest refinement level *l* (the smallest spatial scale) that satisfies

$$t_\ell^{n+1} \leqslant t_{\ell-1}^{n+1}, \quad 0 \leqslant \ell \leqslant \ell_{\max},$$

Conservative and consistent flux evaluation:

Fluxes & jump terms are computed by the fine grid cell at a fine/coarse boundary, and are summed to a memory variable of the coarse grid cell (note that the space-time time boundary integral of the flux is additive).

$$\mathbf{f}_{i+\frac{1}{2},jk} = \frac{1}{\Delta t_\ell}\frac{1}{\Delta y_\ell}\frac{1}{\Delta z_\ell}\sum_{ii=1}^{\mathfrak{r}}\sum_{jj=1}^{\mathfrak{r}}\sum_{kk=1}^{\mathfrak{r}}\int_{\mathcal{T}_{ii}}\int_{\mathcal{Y}_{jj}}\int_{\mathcal{Z}_{kk}}\tilde{\mathbf{f}}(\mathbf{q}_h^-, \mathbf{q}_h^+)\, dz\, dy\, dt,$$

AMR with Time-Accurate Local Time Stepping (LTS)

Within our high order one-step predictor-corrector approach, LTS is *almost* trivial.

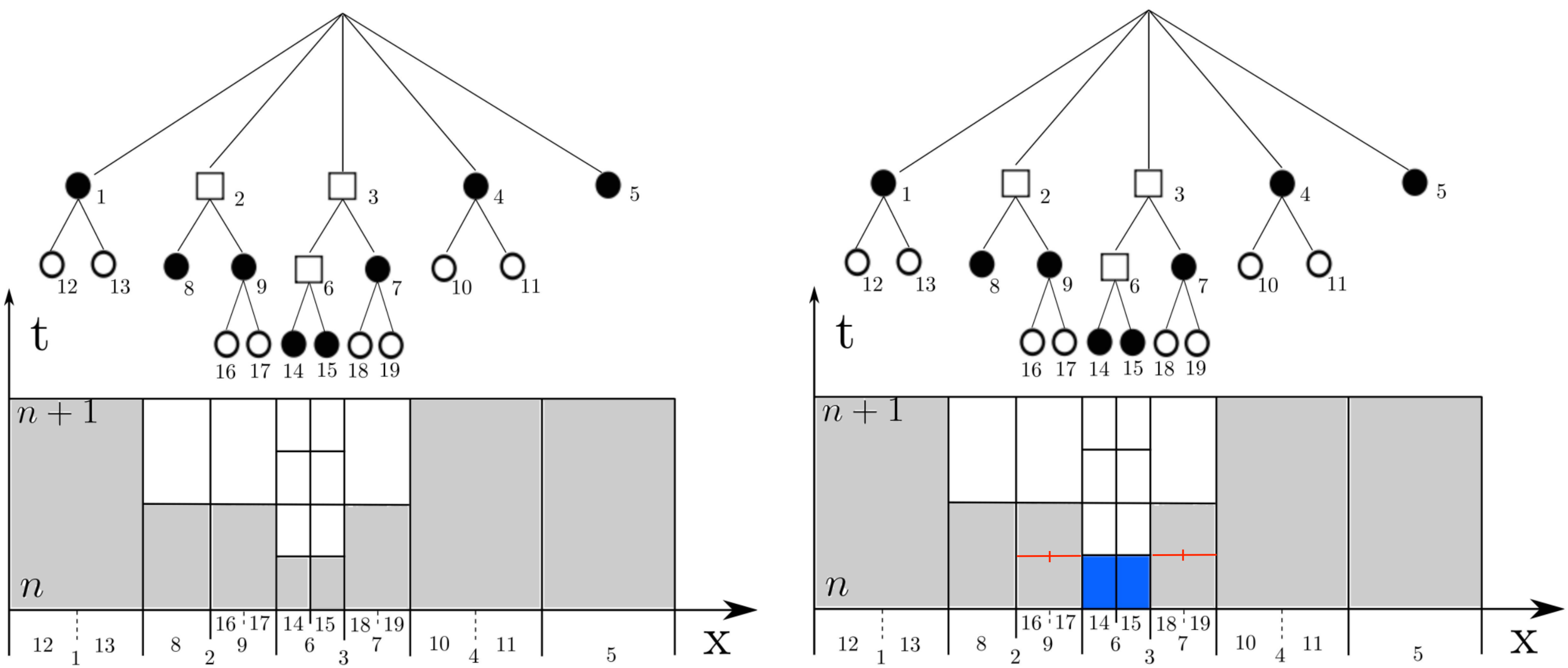

AMR with Time-Accurate Local Time Stepping (LTS)

Within our high order one-step predictor-corrector approach, LTS is *almost* trivial.

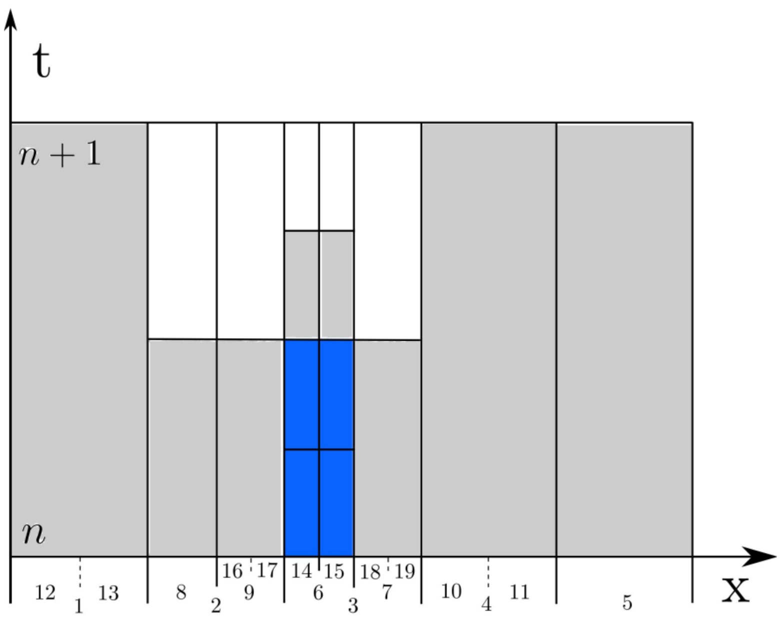

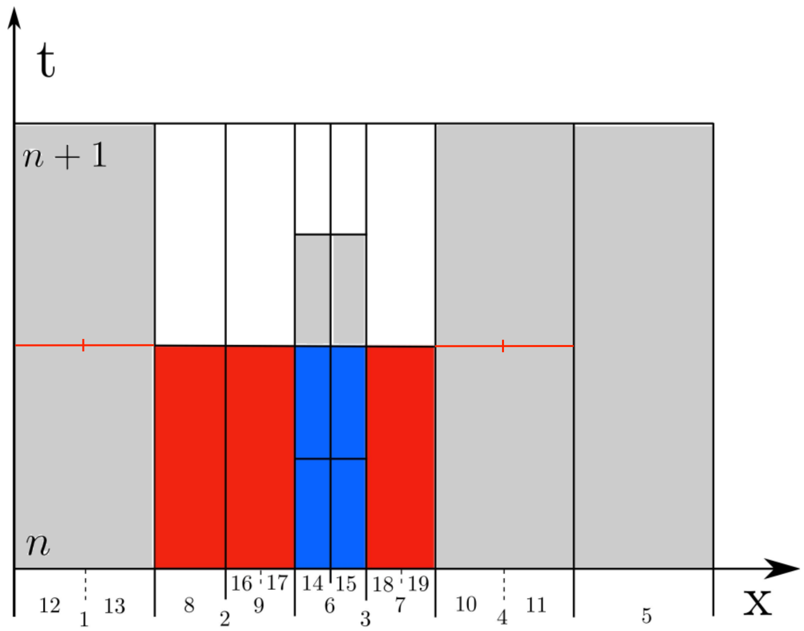

Numerical Convergence Study with AMR

Convergence rates obtained with third and fourth order schemes for a smooth problem solving the compressible BN multiphase model.

$N_G \times N_G$	ϵ_{L_2}	$\mathcal{O}(L_2)$	$N_G \times N_G$	ϵ_{L_2}	$\mathcal{O}(L_2)$
		$\mathcal{O}3$			$\mathcal{O}4$
$15\times15^*$	4.9627E-01		$15\times15^*$	4.6443E-01	
30×30	2.5428E-02	4.29	30×30	2.3166E-02	4.33
45×45	1.3665E-02	3.27	45×45	1.0674E-02	3.43
60×60	7.8621E-03	2.99	60×60	1.0115E-03	4.42
90×90	2.0279E-03	3.07	75×75	5.6484E-04	4.17
120×120	9.9613E-04	2.99	90×90	2.9489E-04	4.11

Table 1
Assessment of the overall efficiency of high order one-step ADER-WENO schemes on space–time adaptive AMR grids ($\mathfrak{r}=4$, $\ell=2$). Normalized average CPU time per real element update with respect to the second order scheme on uniform grid.

Scheme order	Uniform grid	AMR grid	Total AMR overhead
$\mathcal{O}2$	1.00	1.15	15%
$\mathcal{O}3$	3.18	3.82	20%
$\mathcal{O}4$	8.64	10.82	25%

3D Explosion Problem

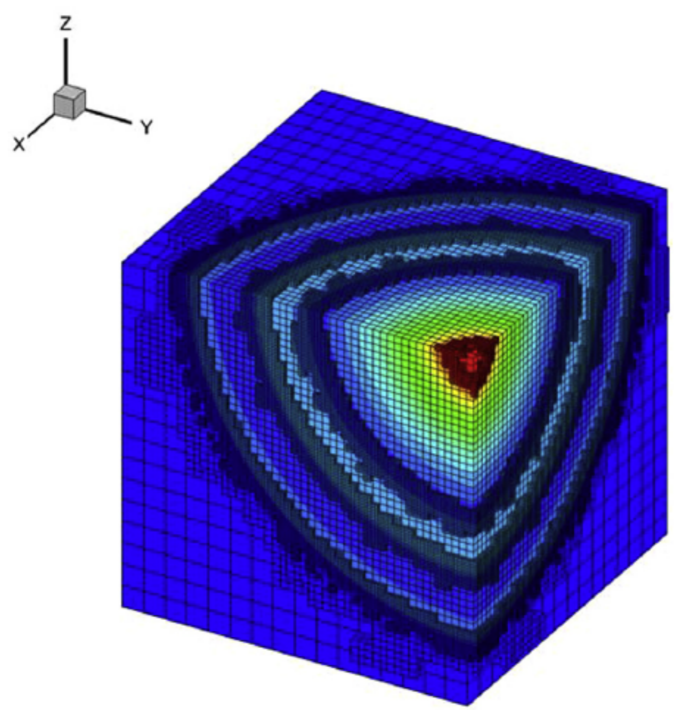

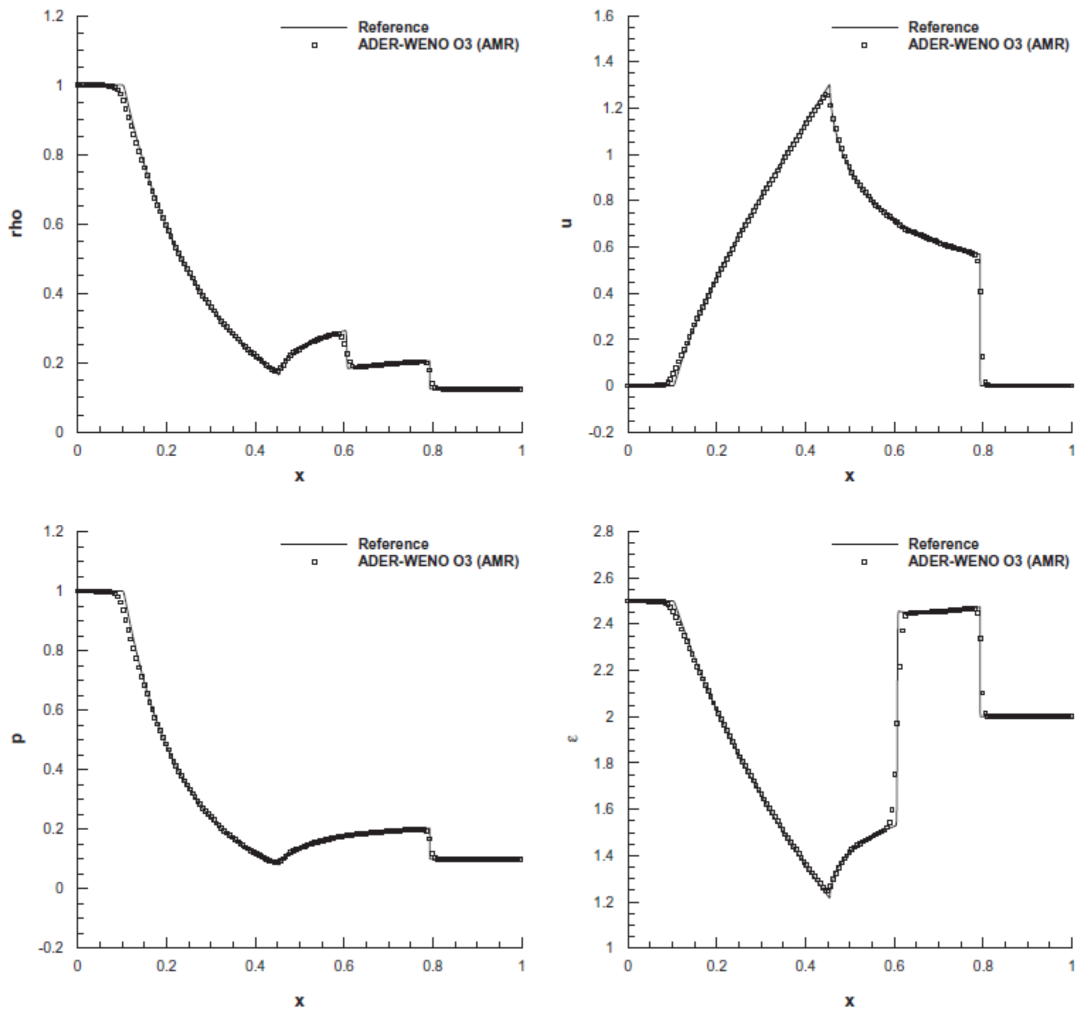

Double Mach Reflection Problem

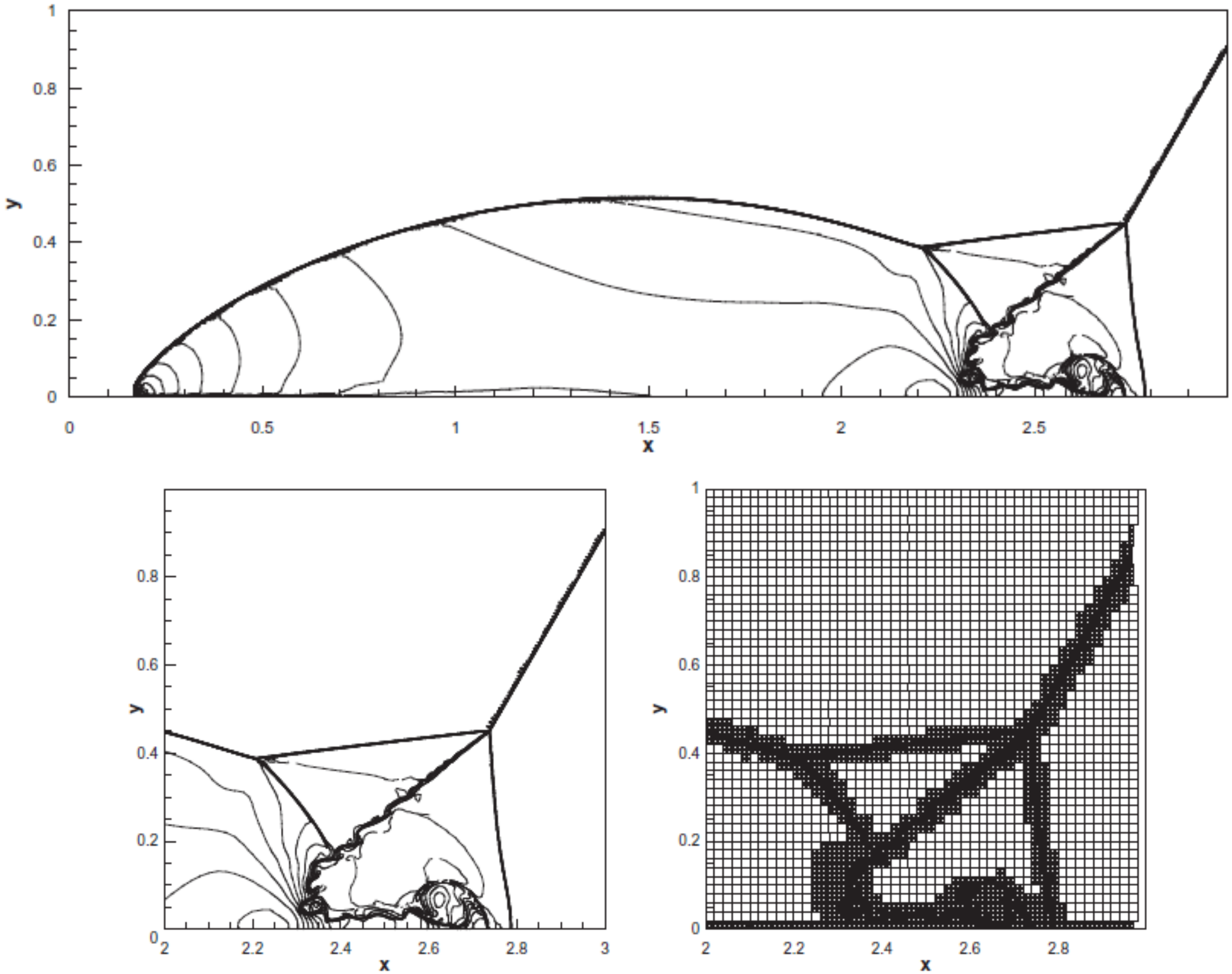

2D Riemann Problems

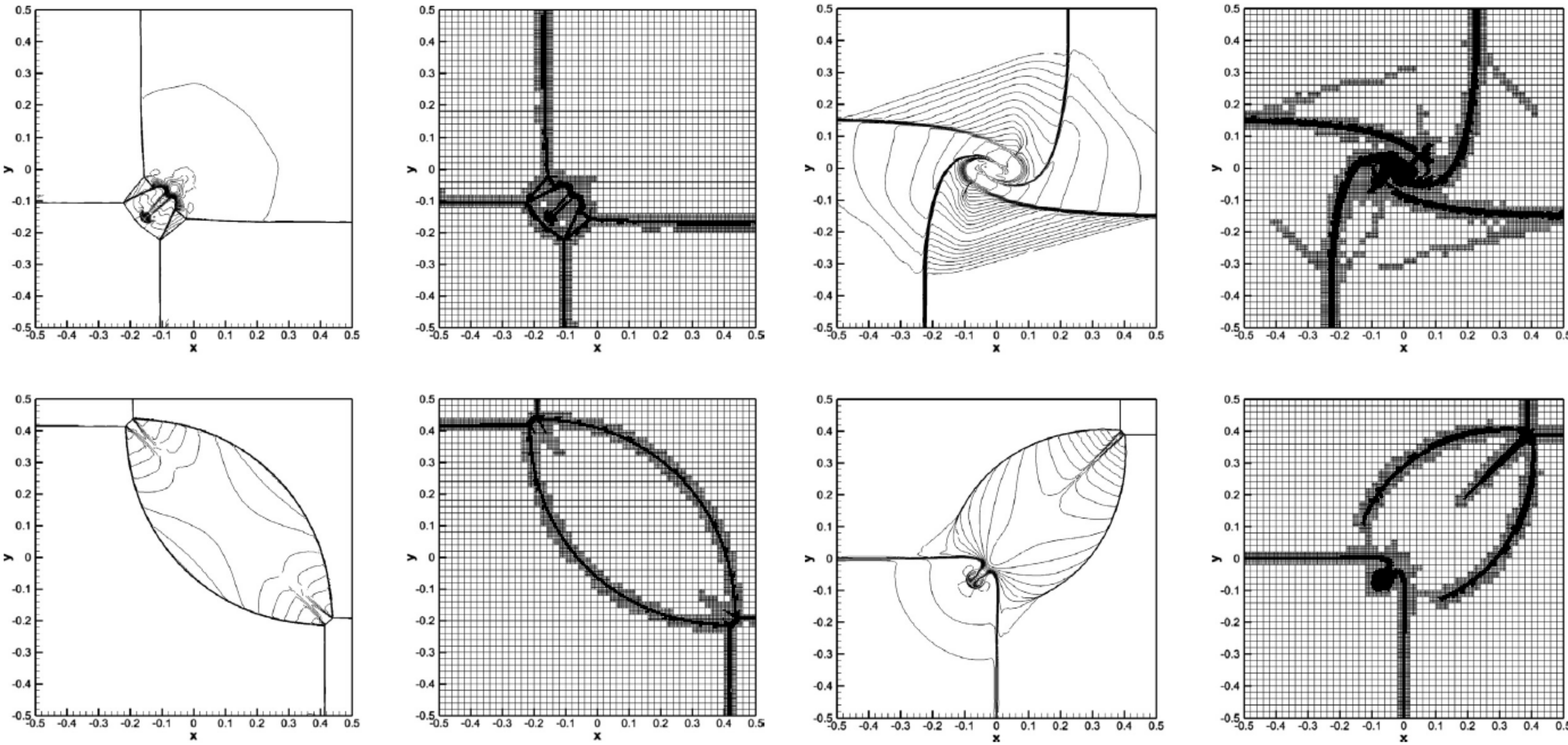

Forward Facing Step Problem

Why one should consider better than third order AMR:

i) less numerical dissipation than AMR based on standard second order TVD schemes

ii) more small-scale flow structures

iii) better preservation of physical features

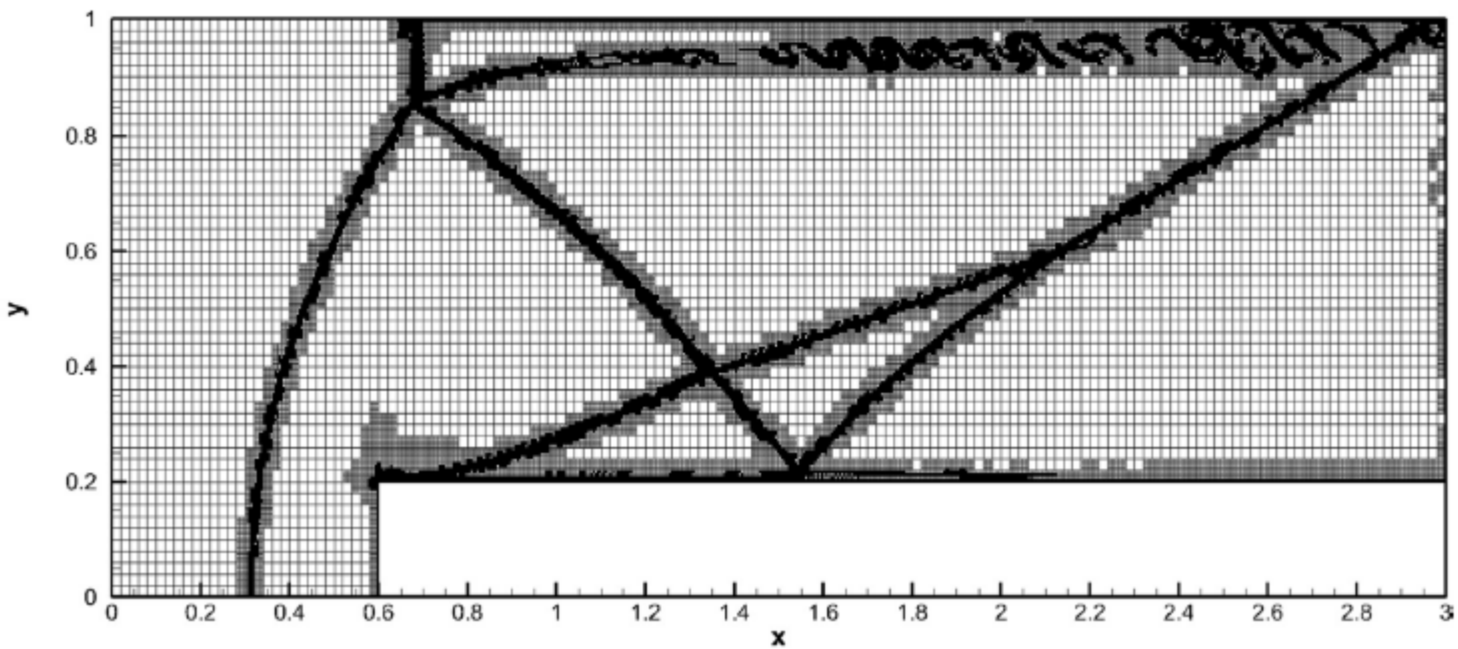

Forward Facing Step Problem

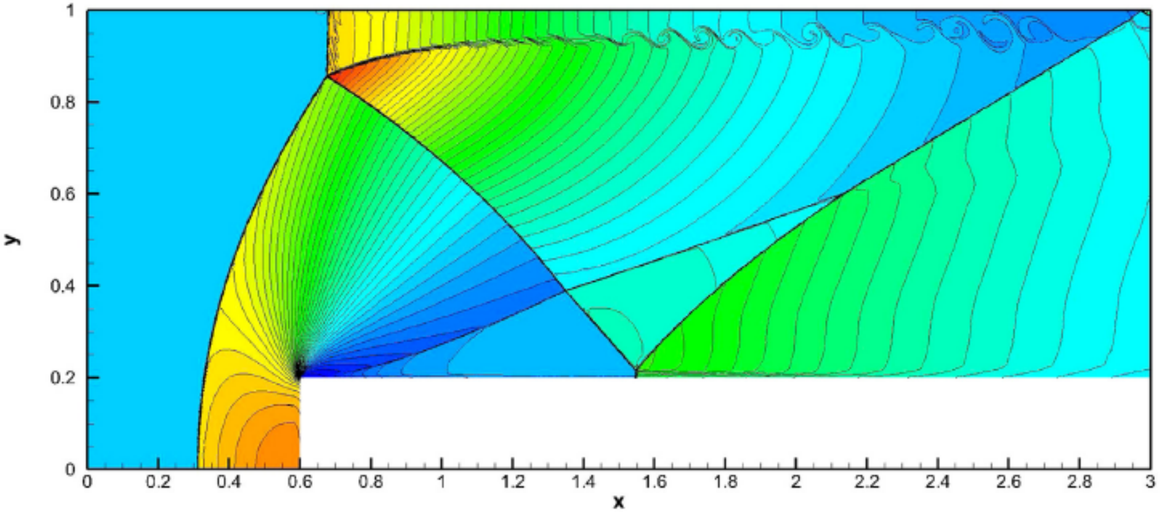

Third order AMR (ADER-WENO) visible rollup

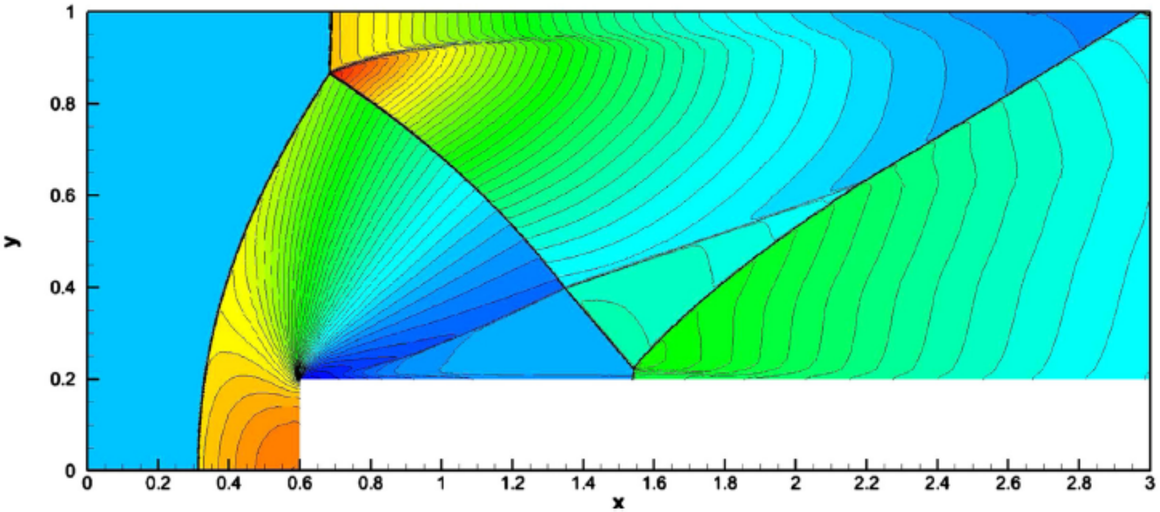

Second order AMR (TVD) no rollup

Sound Generation by a Co-Rotating Vortex Pair

Simple model problem from computational aeroacoustics (CAA)

- Low Mach number problem
- Strong pressure amplitudes within the vortex, very low pressure amplitudes in the sound waves
-Real multi-scale problem (vortex of size 1, acoustic wavelength about 40)
- Computational domain [500 x 500]
- Fourth order AMR scheme
- Three levels of refinement
- about 100.000 elements
- **equivalent** resolution **16000x16000** (256.000.000 cells)

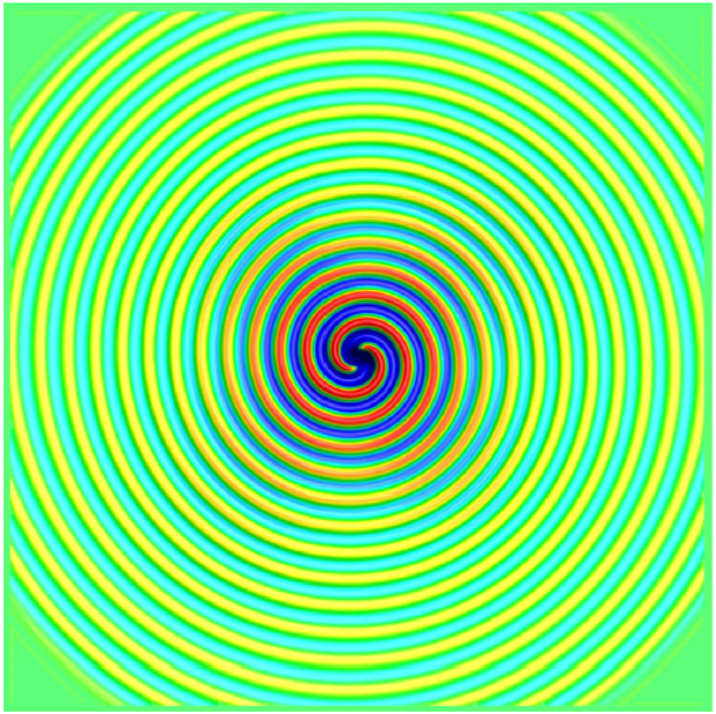

Sound Generation by a Co-Rotating Vortex Pair

An **unphysical** vortex merger is obtained with a second order AMR on a grid that is twice as fine (same number of DOF compared to the fourth order scheme), while the fourth order AMR reproduces the correct solution at the final time t=500.

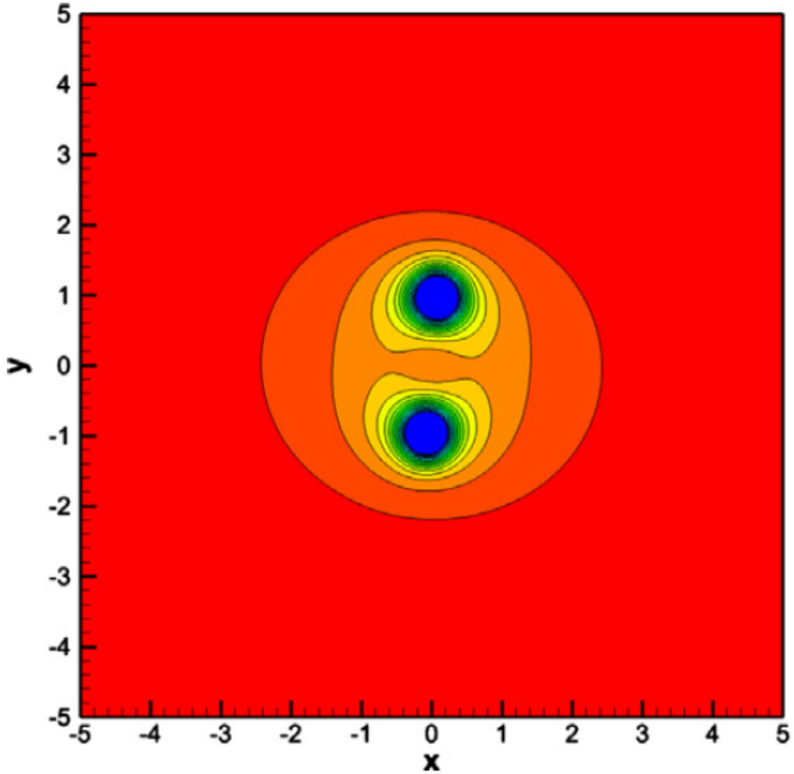

AMR with
fourth order ADER-WENO

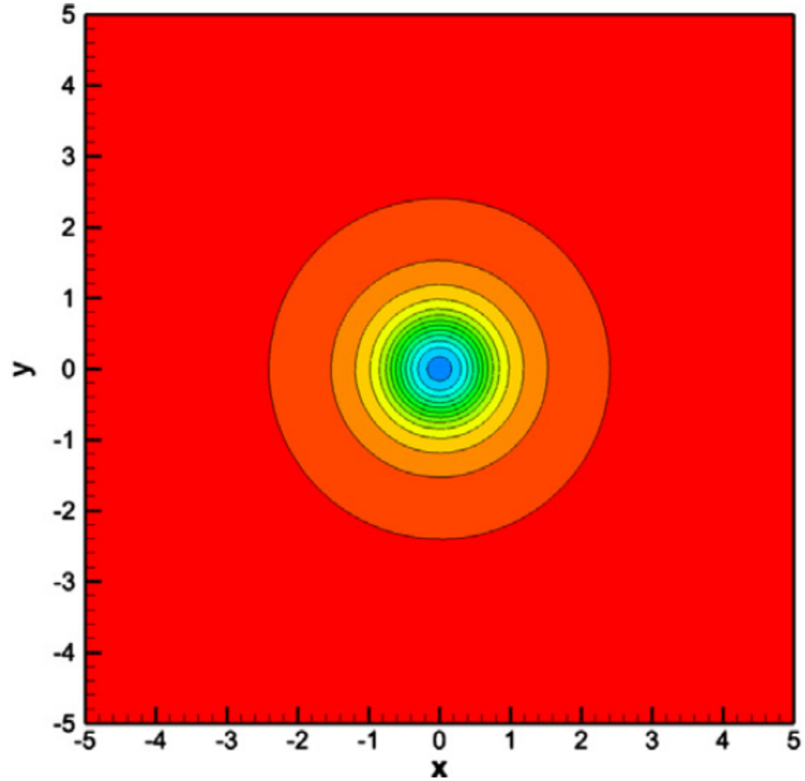

AMR with
second order TVD

Sound Generation by a Co-Rotating Vortex Pair

Unphysical vortex merger with second order AMR on a twice as fine grid (same number of DOF compared to the fourth order scheme)

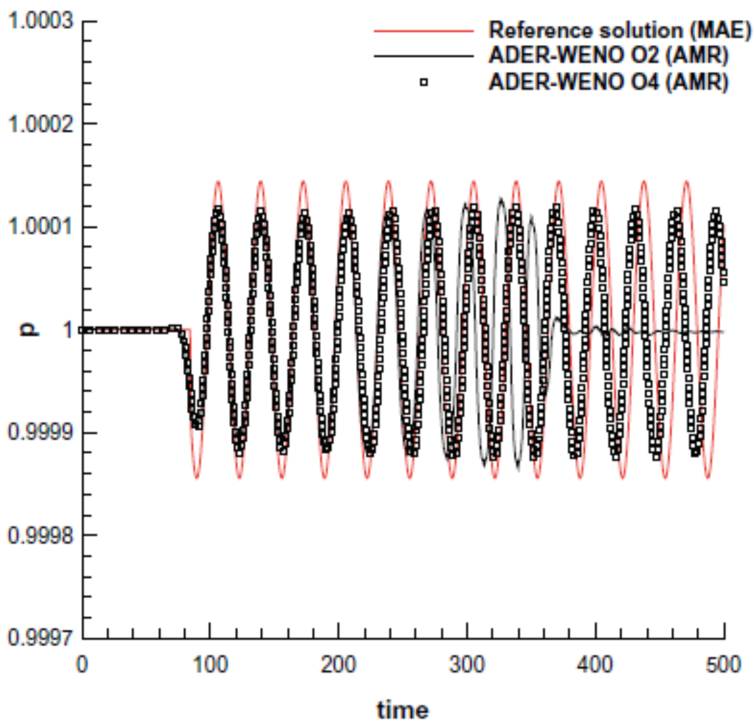

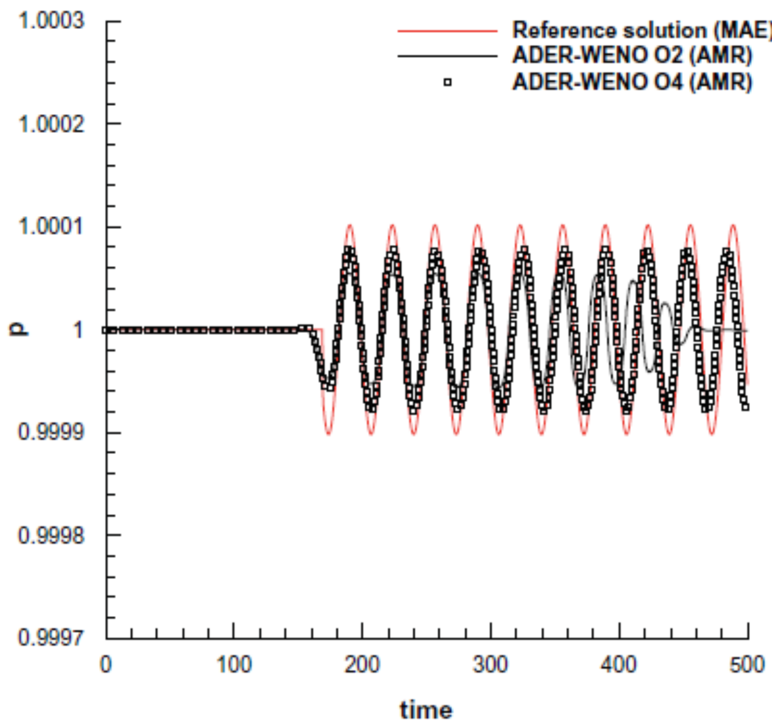

MHD Orszag-Tang Vortex

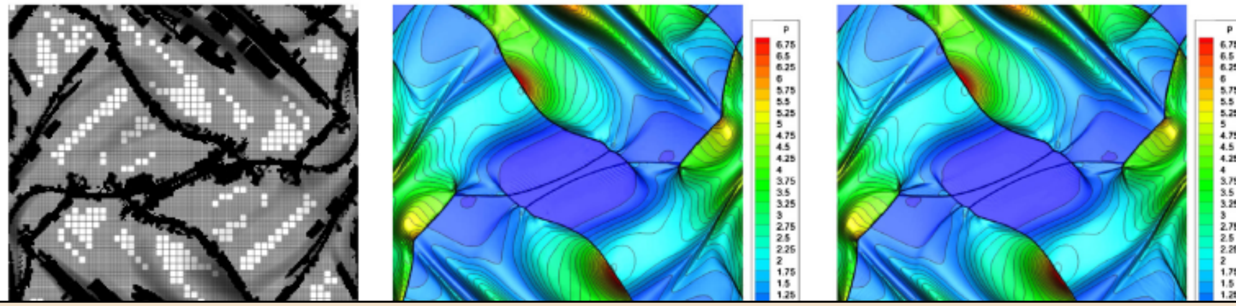

Memory and CPU time comparison of the third order ADER-WENO AMR method and ADER-WENO on a uniform fine grid for the Orszag–Tang problem. Memory consumption is measured in maximum number of elements and CPU time is normalized with respect to the simulation on the fine uniform mesh.

	AMR	Uniform	Ratio
Cells	454,525	640,000	1.41
CPU	0.547	1.0	1.83

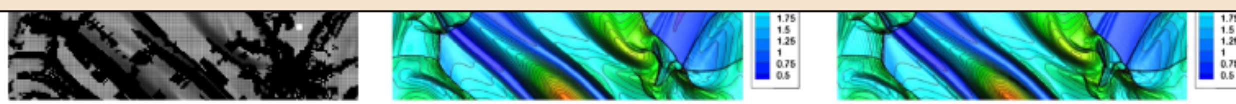

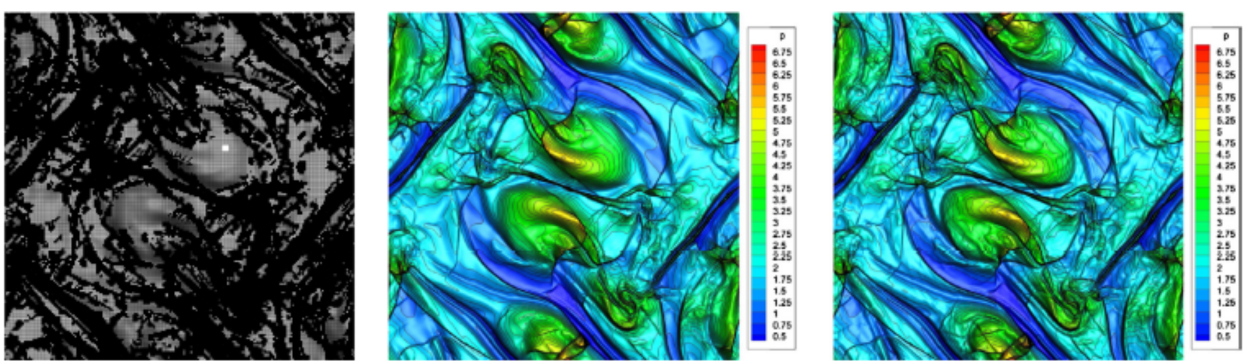

MHD Rotor Problem

Memory and CPU time comparison of the third order ADER-WENO AMR method and ADER-WENO on a uniform fine grid for the MHD rotor problem. Memory consumption is measured in maximum number of elements and CPU time is normalized with respect to the total wallclock time on the uniform mesh.

	AMR	Uniform	Ratio
Elements	179,680	921,600	5.13
CPU time	0.140	1.0	7.14

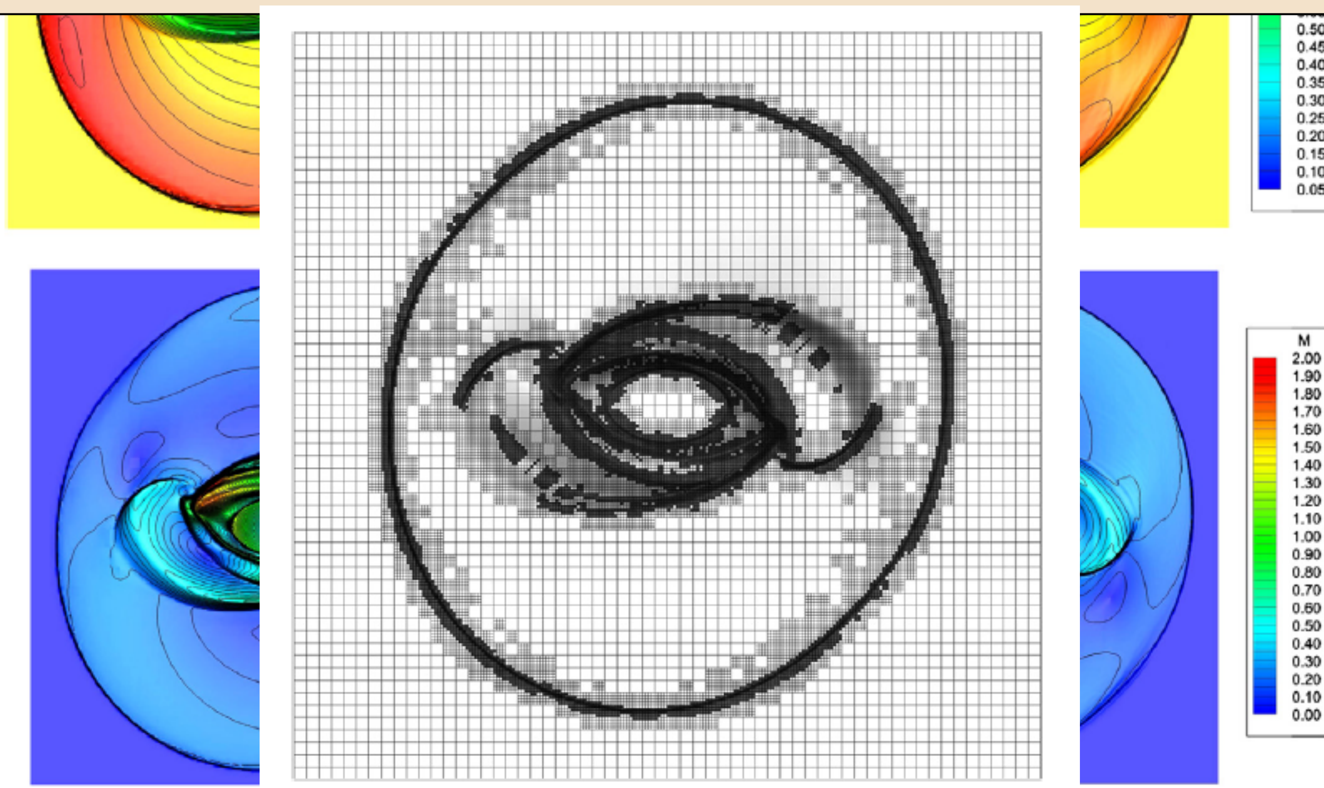

High-Order Lagrangian Schemes on Unstructured Meshes

1. Local Space-Time Galerkin Predictor:

Iso-parametric mapping of the physical space-time-element (left) to the space-time reference element (right)

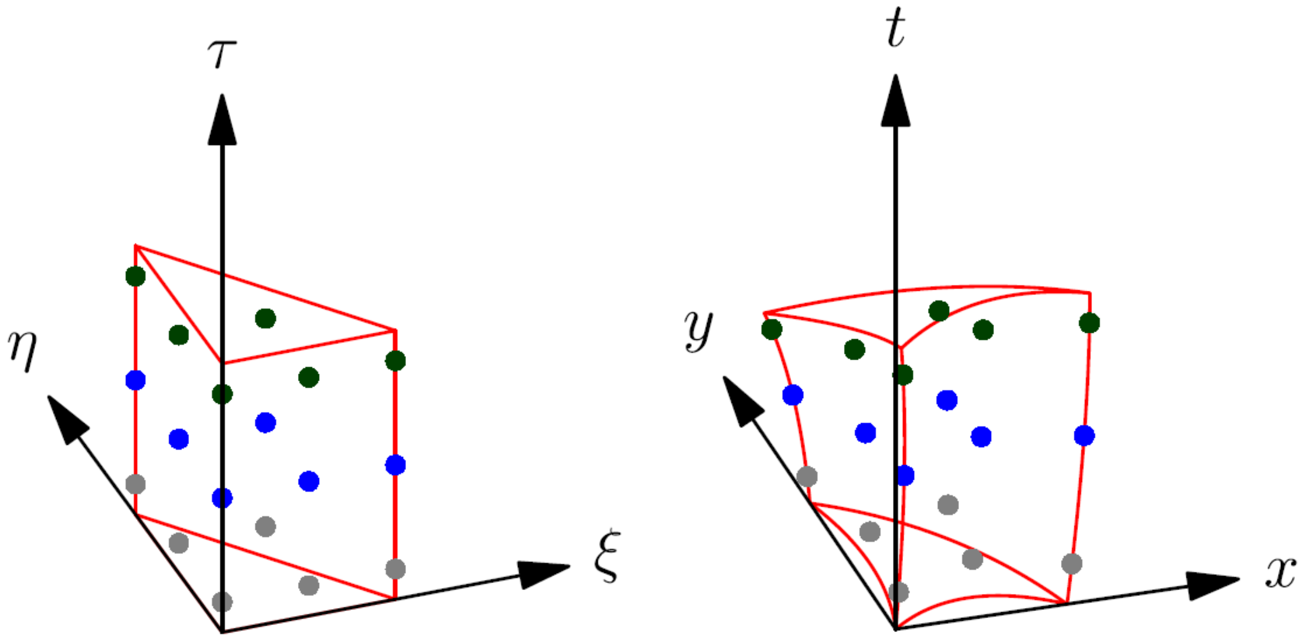

High-Order Lagrangian Schemes on Unstructured Meshes

1. Local Space-Time Galerkin Predictor:

Iso-parametric mapping of the physical space-time-element to the space-time reference element

$$x(\xi,\eta,\tau)=\theta_l(\xi,\eta,\tau)\widehat{x}_{l,i}, \qquad y(\xi,\eta,\tau)=\theta_l(\xi,\eta,\tau)\widehat{y}_{l,i}, \qquad t(\xi,\eta,\tau)=\theta_l(\xi,\eta,\tau)\widehat{t}_l,$$

with the Jacobian matrix and its inverse given by

$$J_{st}=\frac{\partial\tilde{\mathbf{x}}}{\partial\tilde{\boldsymbol{\xi}}}=\begin{pmatrix} x_\xi & x_\eta & x_\tau \\ y_\xi & y_\eta & y_\tau \\ 0 & 0 & \Delta_t \end{pmatrix} \qquad J_{st}^{-1}=\frac{\partial\tilde{\boldsymbol{\xi}}}{\partial\tilde{\mathbf{x}}}=\begin{pmatrix} \xi_x & \xi_y & \xi_t \\ \eta_x & \eta_y & \eta_t \\ 0 & 0 & \frac{1}{\Delta t} \end{pmatrix}$$

PDE in the reference system

$$\frac{\partial\mathbf{Q}}{\partial\tau}+\Delta t\left[\frac{\partial\mathbf{Q}}{\partial\xi}\cdot\frac{\partial\xi}{\partial t}+\left(\frac{\partial\xi}{\partial\mathbf{x}}\right)^T\nabla_\xi\cdot\mathbf{F}+\mathbf{B}(\mathbf{Q})\cdot\left(\frac{\partial\xi}{\partial\mathbf{x}}\right)^T\nabla_\xi\mathbf{Q}\right]=\Delta t\mathbf{S}(\mathbf{Q}),$$

High-Order Lagrangian Schemes on Unstructured Meshes

1. Local Space-Time Galerkin Predictor:

Using the abbreviation

$$\mathbf{H} = \frac{\partial \mathbf{Q}}{\partial \xi} \cdot \frac{\partial \xi}{\partial t} + \left(\frac{\partial \xi}{\partial \mathbf{x}} \right)^T \nabla_\xi \cdot \mathbf{F} + \mathbf{B}(\mathbf{Q}) \cdot \left(\frac{\partial \xi}{\partial \mathbf{x}} \right)^T \nabla_\xi \mathbf{Q},$$

and inserting the discrete space-time solution one obtains the following element local algebraic system:

$$[\theta_k(\xi,1), \theta_l(\xi,1)]^1 \hat{\mathbf{q}}_{l,i} - \left\langle \frac{\partial \theta_k}{\partial \tau}, \theta_l \right\rangle \hat{\mathbf{q}}_{l,i}$$
$$= [\theta_k(\xi,0), \psi_l(\xi)]^0 \hat{\mathbf{w}}^n_{l,i} + \langle \theta_k, \theta_l \rangle \Delta t \left(\widehat{\mathbf{S}}_{l,i} - \widehat{\mathbf{H}}_{l,i} \right).$$

High-Order Lagrangian Schemes on Unstructured Meshes

1. Local Space-Time Galerkin Predictor:

Space-time predictor solution of the local mesh velocity:

$$\frac{d\mathbf{x}}{dt} = \mathbf{V}(x,y,t), \qquad \mathbf{V}_h = \mathbf{V}_h(\xi,\eta,\tau) = \theta_l(\xi,\eta,\tau)\widehat{\mathbf{V}}_{l,i},$$

$$\left\langle \theta_k, \frac{\partial \theta_l}{\partial \tau} \right\rangle \widehat{\mathbf{x}}_{l,i} = \Delta t \left\langle \theta_k, \theta_l \right\rangle \widehat{\mathbf{V}}_{l,i},$$

2. Node update (average according to Cheng & Shu, or...)

$$\overline{\mathbf{V}}_k^n = \frac{1}{N_k} \sum_{T_j^n \in \mathcal{V}_k} \overline{\mathbf{V}}_{k,j}^n, \qquad \text{with} \qquad \overline{\mathbf{V}}_{k,j}^n = \left(\int_0^1 \theta_l(\xi_{e,m(k)}, \eta_{e,m(k)}, \tau) d\tau \right) \widehat{\mathbf{V}}_{l,j}.$$

$$\mathbf{X}_k^{n+1} = \mathbf{X}_k^n + \Delta t \overline{\mathbf{V}}_k^n,$$

Node Solvers

1. Cheng & Shu :

Simple arithmetic average. No upwinding!

2. Maire (2011), Després:

In a cell-centered Lagrangian framework, the computation of the velocity at the mesh vertices <u>requires</u> the solution of a multi-dimensional Riemann problem, or something equivalent.

(Balsara 2010, 2012, Balsara et al. 2013)

Integrate the conservation law over an expanding 3D space-time control volume and extract a multi-d HLL averaged state, which determines the mesh velocity.

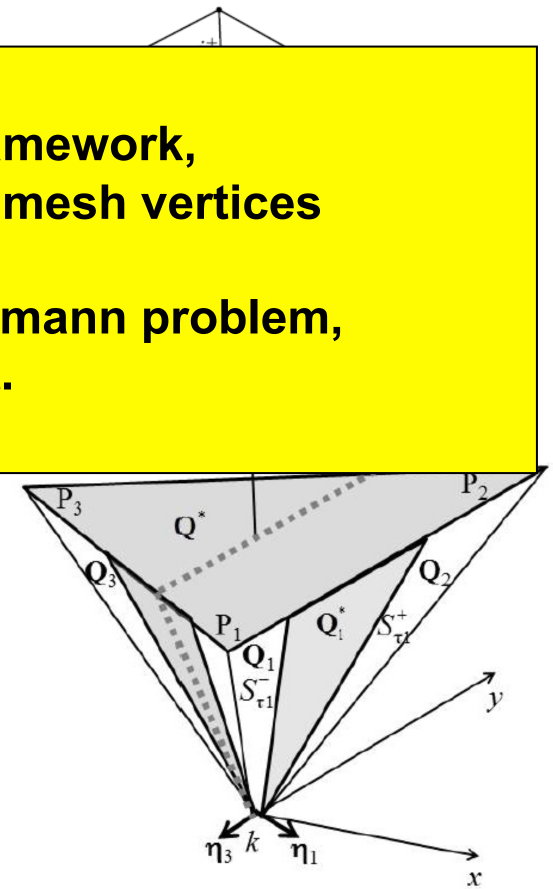

High-Order Lagrangian Schemes on Unstructured Meshes

3. Finite Volume Scheme

Formulation in space-time:

$$\tilde{\nabla} \cdot \widetilde{\mathbf{F}} + \widetilde{\mathbf{B}}(\mathbf{Q}) \cdot \tilde{\nabla}\mathbf{Q} = \mathbf{S}(\mathbf{Q})$$

$$\tilde{\nabla} = \left(\frac{\partial}{\partial x}, \frac{\partial}{\partial y}, \frac{\partial}{\partial t} \right)^T \qquad \widetilde{\mathbf{F}} = (\mathbf{f}, \ \mathbf{g}, \ \mathbf{Q}) \qquad \widetilde{\mathbf{B}} = (\mathbf{B}_1, \mathbf{B}_2, 0)$$

Integration over a space-time control volume yields

$$\int_{C_i^n} \tilde{\nabla} \cdot \widetilde{\mathbf{F}} \ d\mathbf{x}dt + \int_{C_i^n} \widetilde{\mathbf{B}}(\mathbf{Q}) \cdot \tilde{\nabla}\mathbf{Q} \ d\mathbf{x}dt = \int_{C_i^n} \mathbf{S}(\mathbf{Q}) \ d\mathbf{x}dt.$$

Integration by parts of the flux and integration of the non-conservative product:

$$\int_{\partial C_i^n} (\widetilde{\mathbf{F}} + \tilde{\mathbf{D}}) \cdot \ \tilde{\mathbf{n}} \ dS + \int_{C_i^n \backslash \partial C_i^n} \widetilde{\mathbf{B}}(\mathbf{Q}) \cdot \tilde{\nabla}\mathbf{Q} \ d\mathbf{x}dt = \int_{C_i^n} \mathbf{S}(\mathbf{Q}) \ d\mathbf{x}dt,$$

High-Order Lagrangian Schemes on Unstructured Meshes

3. Finite Volume Scheme

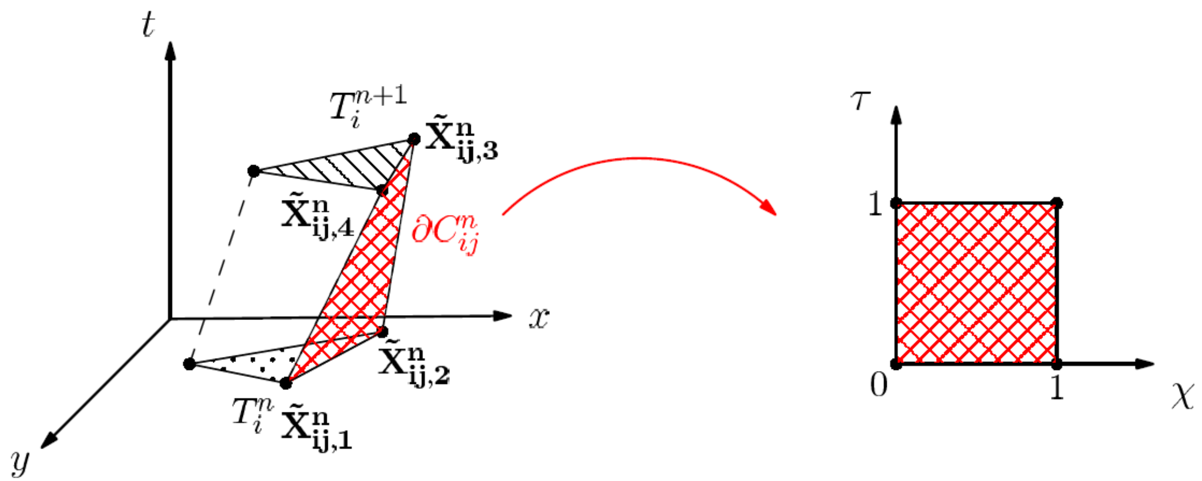

Geometric conservation law (**GCL**) satisfied **by construction**:

$$\int_{\partial C_i^n} \tilde{\mathbf{n}} \, dS = 0.$$

Bi-linear parametrization of the space time faces

$$\partial C_{ij}^n = \tilde{\mathbf{x}}(\chi,\tau) = \sum_{k=1}^{4} \beta_k(\chi,\tau)\,\tilde{\mathbf{X}}_{ij,k}^n, \qquad 0 \le \chi \le 1, \quad 0 \le \tau \le 1,$$

High-Order Lagrangian Schemes on Unstructured Meshes

3. Finite Volume Scheme

Path-conservative approach [Parés 2006, Castro et al. 2006] for the non-conservative jump terms:

$$\tilde{\mathbf{D}} \cdot \tilde{\mathbf{n}} = \frac{1}{2}\left(\int_0^1 \tilde{\mathbf{B}}(\boldsymbol{\Psi}(\mathbf{Q}^-, \mathbf{Q}^+, s)) \cdot \tilde{\mathbf{n}} \; ds \right) (\mathbf{Q}^+ - \mathbf{Q}^-)$$

Final high-order one-step ALE Finite volume scheme:

$$|T_i^{n+1}| \; \mathbf{Q}_i^{n+1} = |T_i^n| \; \mathbf{Q}_i^n - \sum_{T_j \in \mathcal{N}_i} \int_0^1 \int_0^1 |\partial C_{ij}^n| \tilde{\mathbf{G}}_{ij} \, d\chi d\tau + \int_{\mathcal{C}_i^n \setminus \partial \mathcal{C}_i^n} (\mathbf{S}_h - \mathbf{P}_h) \; d\mathbf{x}dt$$

Osher-type scheme:

$$\tilde{\mathbf{G}}_{ij} = \frac{1}{2}\left(\tilde{\mathbf{F}}(\mathbf{q}_h^+) + \tilde{\mathbf{F}}(\mathbf{q}_h^-) \right) \cdot \tilde{\mathbf{n}}_{ij} + \frac{1}{2}\left(\int_0^1 \left(\tilde{\mathbf{B}}(\boldsymbol{\Psi}) \cdot \tilde{\mathbf{n}} - \left| \tilde{\mathbf{A}}_{\tilde{\mathbf{n}}}(\boldsymbol{\Psi}) \right| \right) \; ds \right) (\mathbf{q}_h^+ - \mathbf{q}_h^-)$$

Direct One-Step ALE with Rezoning

The present formulation allows for **rezoning without remapping**, in a consistent, conservative and high order manner:

Reconstruction

Time-Evolution

Node solver

Preliminary mesh at time t^{n+1}

Rezoning and final mesh at time t^{n+1}

One-step time update of the discrete solution to time t^{n+1} using the high-order space-time formalism.

Numerical Convergence Results (MHD Vortex)

Time t = 1.0

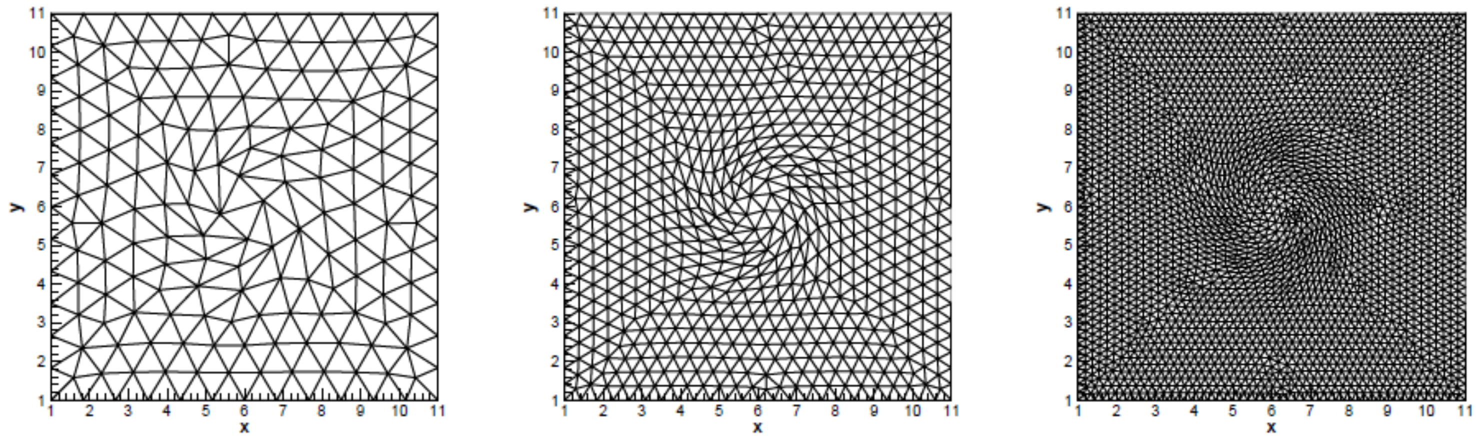

Time t = 2.0

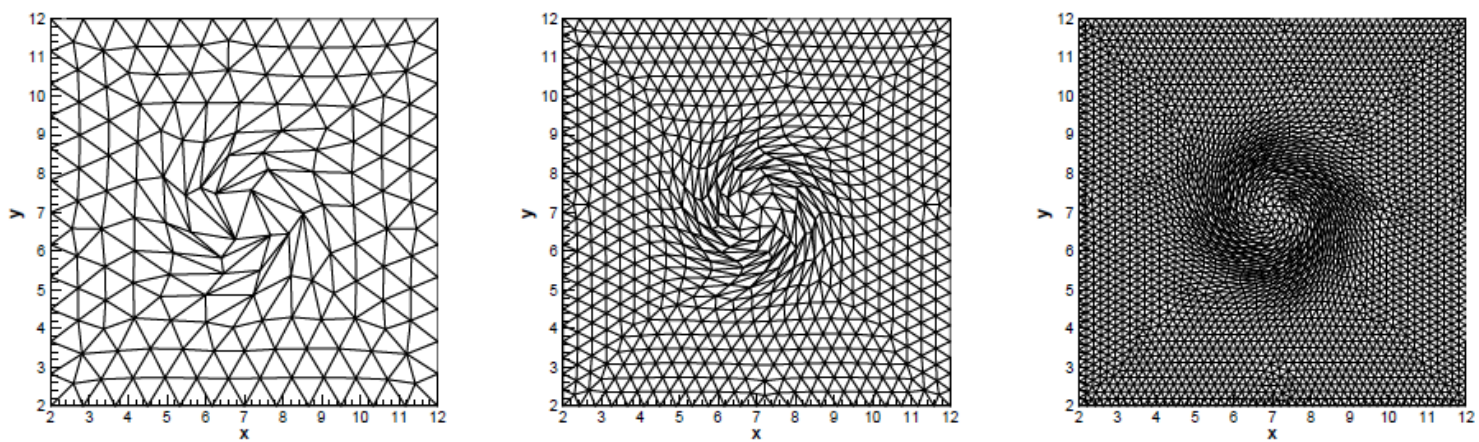

Numerical Convergence Results (MHD Vortex)

	$\mathcal{NS}_{cs}$			$\mathcal{NS}_m$			$\mathcal{NS}_b$	
$h(\Omega(t_f))$	ϵ_{L_2}	$\mathcal{O}(L_2)$	$h(\Omega, t_f)$	ϵ_{L_2}	$\mathcal{O}(L_2)$	$h(\Omega, t_f)$	ϵ_{L_2}	$\mathcal{O}(L_2)$
				$\mathcal{O}1$				
3.26E-01	2.7330E-03	-	3.25E-01	2.7059E-03	-	3.26E-01	2.7381E-03	-
2.37E-01	2.0111E-03	0.96	2.35E-01	2.0173E-03	0.90	2.35E-01	2.0173E-03	0.93
1.64E-01	1.3081E-03	1.17	1.64E-01	1.3055E-03	1.20	1.64E-01	1.3113E-03	1.20
1.28E-01	9.5497E-04	1.26	1.28E-01	9.5150E-04	1.30	1.28E-01	9.5617E-04	1.28
				$\mathcal{O}2$				
3.26E-01	4.8091E-03	-	3.27E-01	4.7707E-03	-	3.26E-01	5.5971E-03	-
2.35E-01	2.8382E-03	1.61	2.37E-01	2.8571E-03	1.58	2.35E-01	2.7874E-03	2.13
1.64E-01	1.4212E-03	1.91	1.63E-01	1.4239E-03	1.88	1.63E-01	1.3789E-03	1.94
1.28E-01	6.4686E-04	3.24	1.28E-01	6.4610E-04	3.26	1.28E-01	7.2141E-04	2.67
				$\mathcal{O}3$				
3.25E-01	1.1417E-03	-	3.25E-01	1.1376E-03	-	3.26E-01	1.1265E-03	-
2.36E-01	1.8935E-04	5.57	2.36E-01	1.8930E-04	5.56	2.36E-01	1.8632E-04	5.56
1.63E-01	7.1734E-05	2.65	1.63E-01	7.1740E-05	2.65	1.63E-01	7.1912E-05	2.60
1.28E-01	3.1651E-05	3.38	1.28E-01	3.1653E-05	3.38	1.28E-01	3.1738E-05	3.38
				$\mathcal{O}4$				
3.26E-01	2.4858E-04	-	3.26E-01	2.4864E-04	-	3.26E-01	2.4472E-04	-
2.35E-01	7.9871E-05	3.50	2.35E-01	7.9875E-05	3.50	2.35E-01	7.9884E-05	3.45
1.63E-01	2.1790E-05	3.55	1.63E-01	2.1791E-05	3.55	1.63E-01	2.1795E-05	3.55
1.28E-01	8.2013E-06	4.03	1.28E-01	8.2014E-06	4.03	1.28E-01	8.1998E-06	4.03
				$\mathcal{O}5$				
3.26E-01	1.2010E-04	-	3.26E-01	1.2010E-04	-	3.26E-01	1.1992E-04	-
2.35E-01	2.7365E-05	4.56	2.35E-01	2.7359E-05	4.56	2.35E-01	2.7327E-05	4.56
1.63E-01	4.8779E-06	4.71	1.63E-01	4.8778E-06	4.71	1.63E-01	4.8898E-06	4.70
1.28E-01	1.3947E-06	5.17	1.28E-01	1.3947E-06	5.17	1.28E-01	1.3935E-06	5.18

Saltzmann Problem

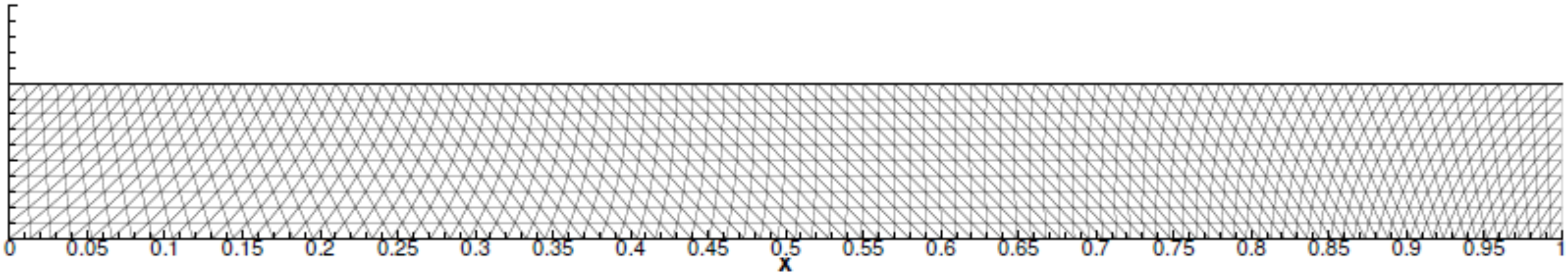

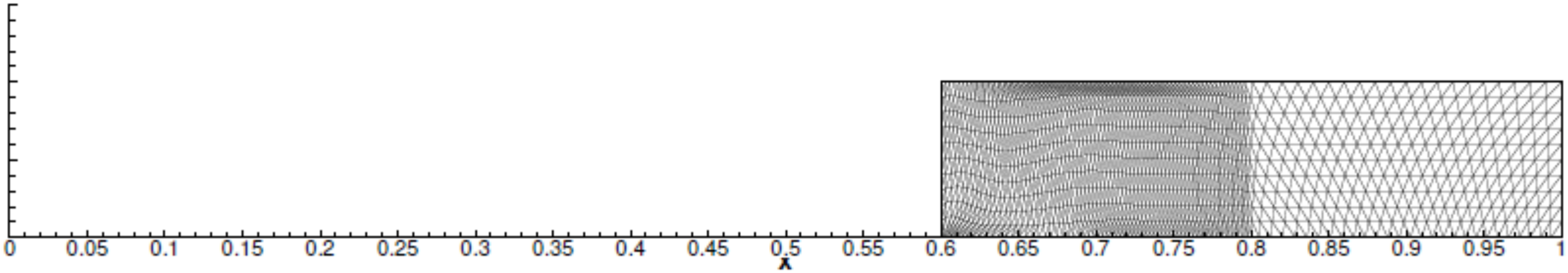

Saltzmann Problem

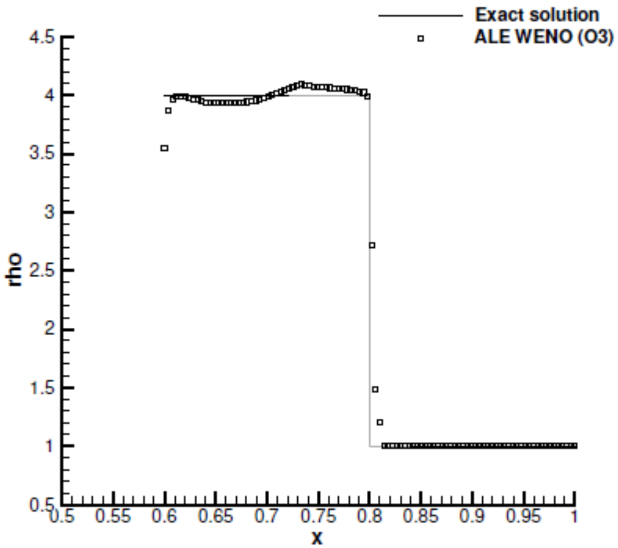

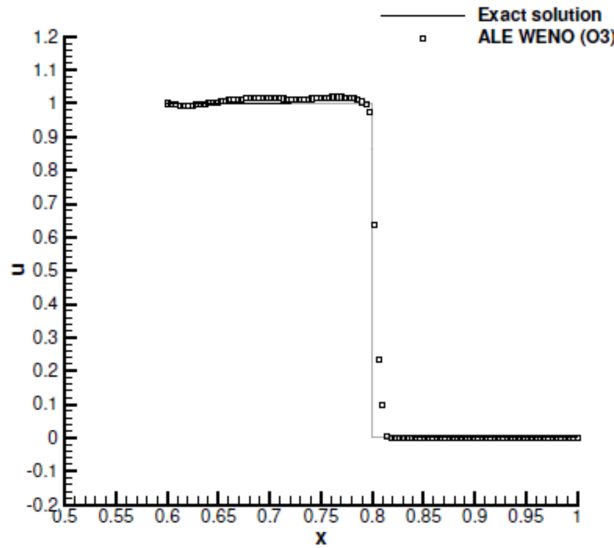

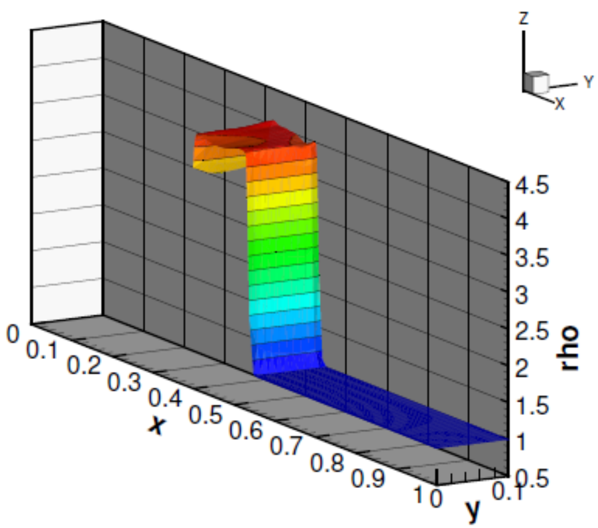

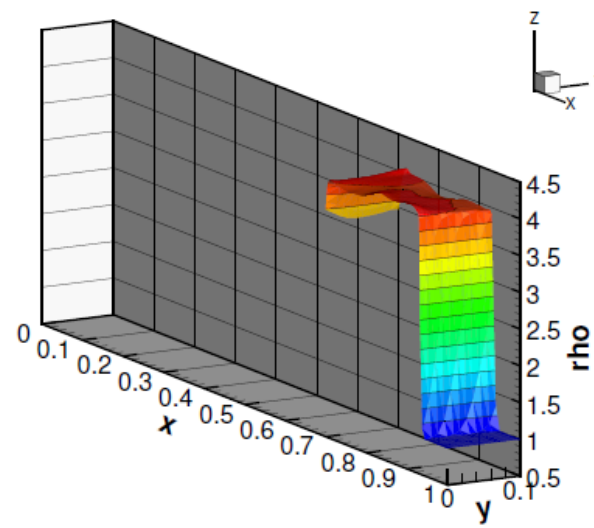

Sedov Problem

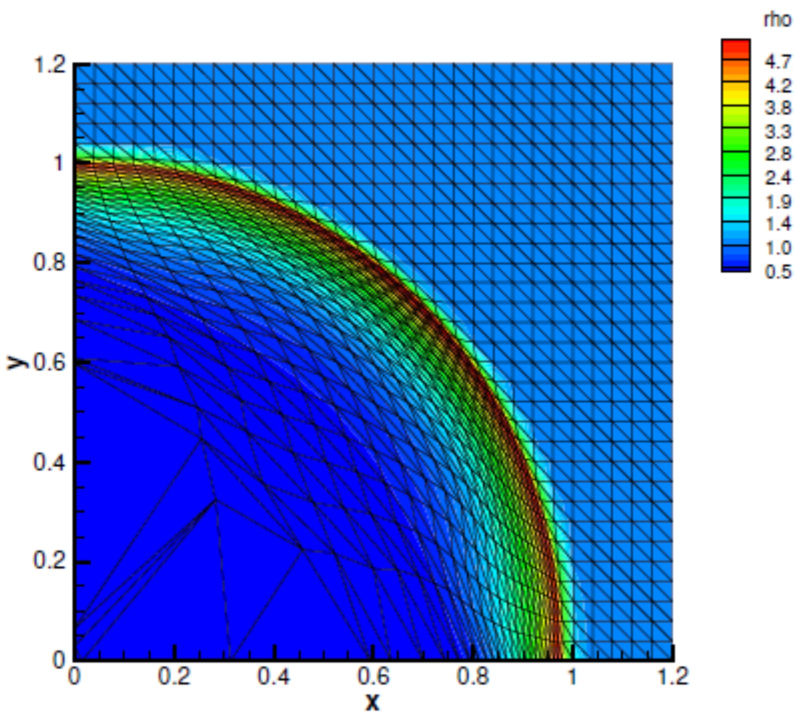

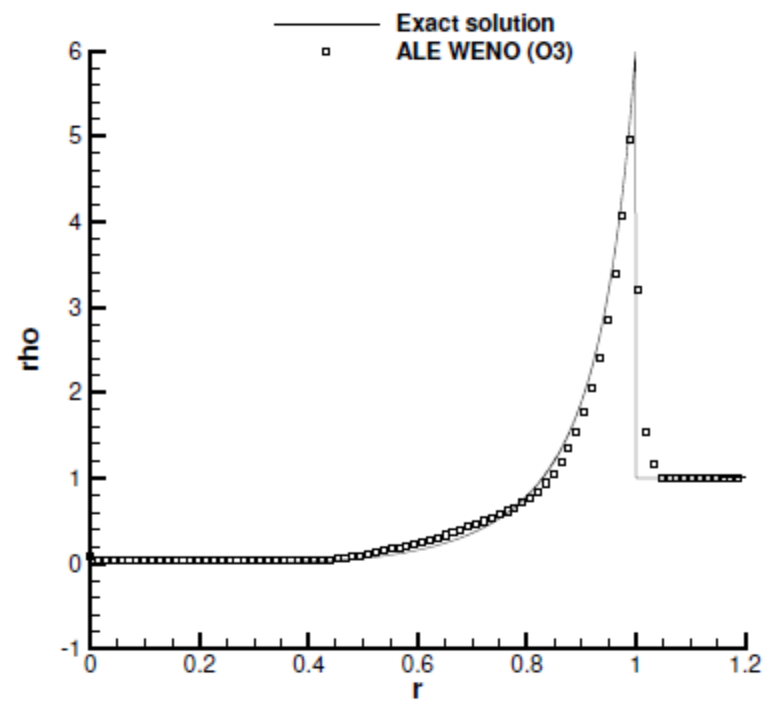

MHD Rotor

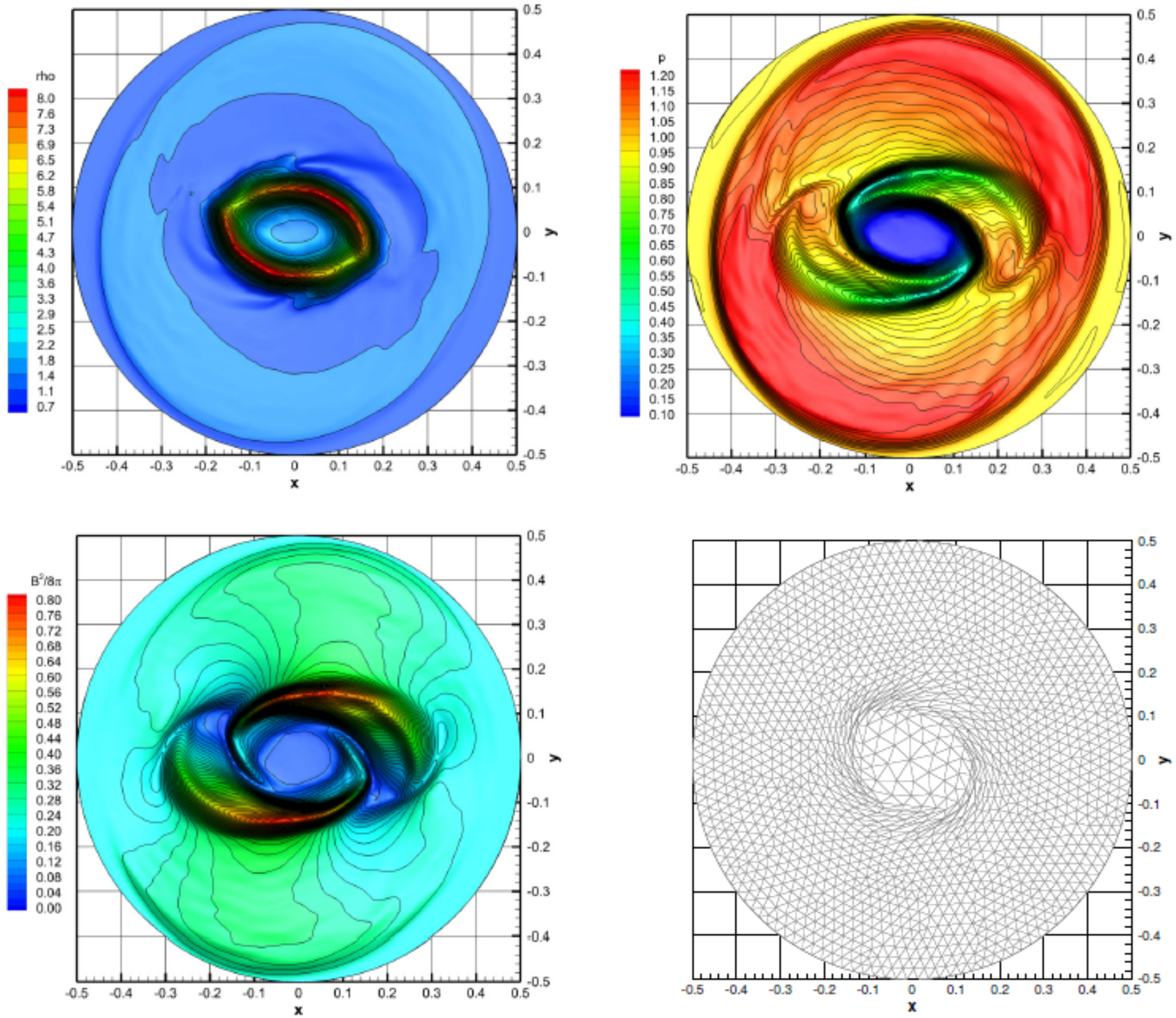
rho
8.0
7.6
7.3
6.9
6.5
6.2
5.8
5.4
5.1
4.7
4.3
4.0
3.6
3.3
2.9
2.5
2.2
1.8
1.4
1.1
0.7
p
1.20
1.15
1.10
1.05
1.00
0.95
0.90
0.85
0.80
0.75
0.70
0.65
0.60
0.55
0.50
0.45
0.40
0.35
0.30
0.25
0.20
0.15
0.10
B²/8π
0.80
0.76
0.72
0.68
0.64
0.60
0.56
0.52
0.48
0.44
0.40
0.36
0.32
0.28
0.24
0.20
0.16
0.12
0.08
0.04
0.00
x
y

MHD Blast Wave

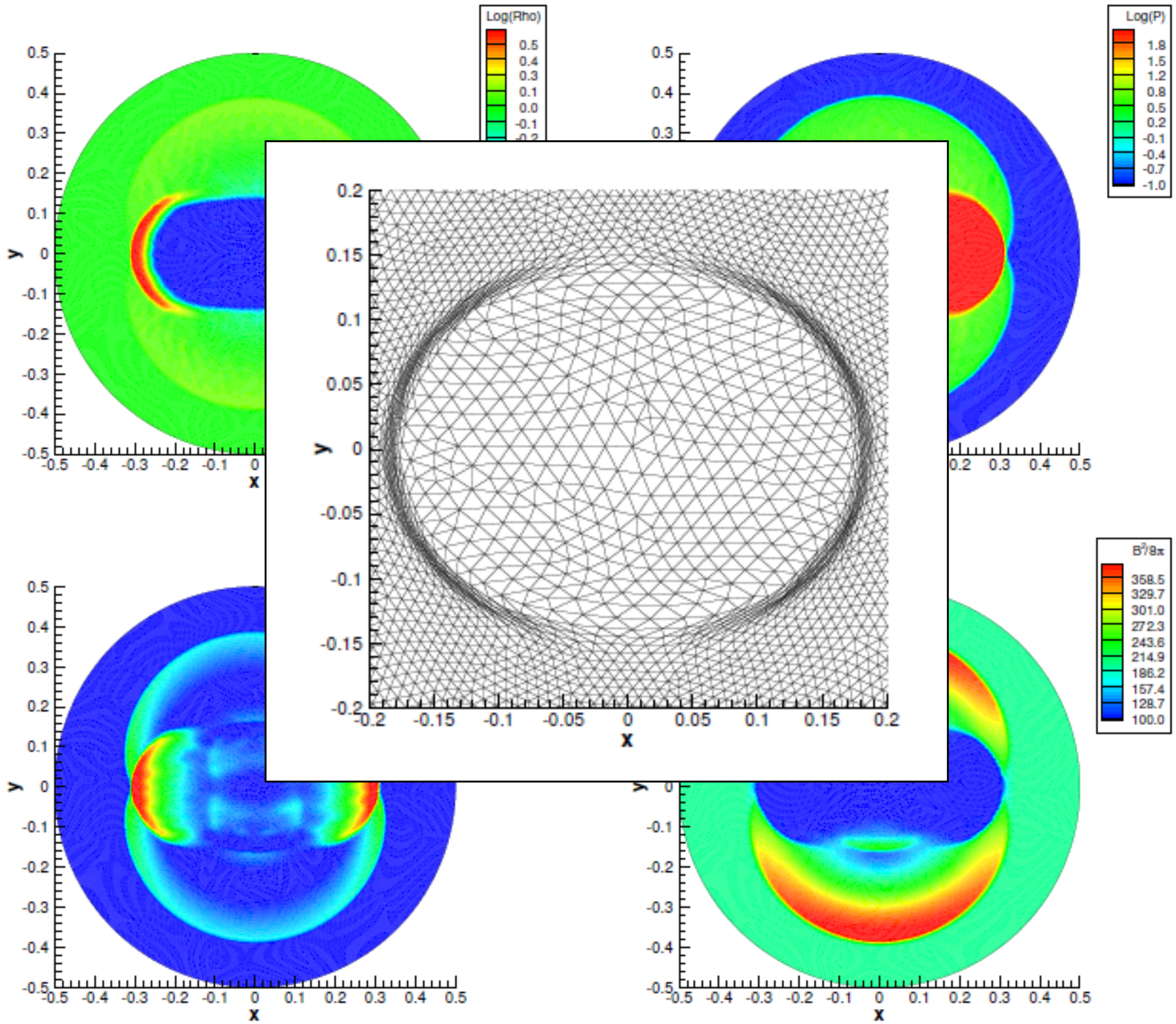

Conclusions

- High order accurate schemes for the solution of very general time-dependent PDE on unstructured meshes in multiple space dimensions.
- High order **finite volume** and **DG** schemes are **special cases** of the new general class of reconstructed $P_N P_M$ DG schemes
- Extension to space-time adaptive Cartesian grids
- Extension to unstructured moving meshes
- Use of multi-dimensional Riemann solver to compute the vertex velocity in the ALE framework.

Still interested in high order methods?

Home | Winter School on Numerical Methods

Contacts Download printable version

Winter School on Numerical Methods

Venue: Department of Civil, Environmental and Mechanical Engineering, Trento (Italy)

Hyperbolic Equations and Applications

Lecturers:

- Prof. Eleuterio Toro OBE, PhD, DhC
- Prof. Ing. Michael Dumbser, PhD

February 3rd - 14th, 2014

Visit www.unitn.it/event/nm2014

The Baer-Nunziato Model of Compressible Multi-Phase Flows

$$\frac{\partial}{\partial t}(\alpha_1\rho_1) + \nabla\cdot(\alpha_1\rho_1\vec{v}_1) = 0,$$

$$\frac{\partial}{\partial t}(\alpha_1\rho_1\vec{v}_1) + \nabla\cdot(\alpha_1(\rho_1\vec{v}_1\vec{v}_1 + p_1)) - p_I\nabla\alpha_1 = 0,$$

$$\boxed{p_I = p_2}$$

$$\frac{\partial}{\partial t}(\alpha_1\rho_1 E_1) + \nabla\cdot(\alpha_1\vec{v}_1(\rho_1 E_1 + p_1)) + p_I\frac{\partial}{\partial t}\alpha_1 = 0,$$

$$\frac{\partial}{\partial t}(\alpha_2\rho_2) + \nabla\cdot(\alpha_2\rho_2\vec{v}_2) = 0,$$

$$\frac{\partial}{\partial t}(\alpha_2\rho_2\vec{v}_2) + \nabla\cdot(\alpha_2(\rho_2\vec{v}_2\vec{v}_2 + p_2)) - p_I\nabla\alpha_2 = 0,$$

$$\frac{\partial}{\partial t}(\alpha_2\rho_2 E_2) + \nabla\cdot(\alpha_2\vec{v}_2(\rho_2 E_2 + p_2)) + p_I\frac{\partial}{\partial t}\alpha_2 = 0,$$

$$\frac{\partial}{\partial t}\alpha_1 + \vec{v}_I\cdot\nabla\alpha_1 = 0,$$

$$\boxed{\vec{v}_I = \vec{v}_1}$$

Special Case of the Baer-Nunziato Model

For the gas phase, we suppose *p*=0=const. and the liquid phase is modeled by the usual Tait equation of state (weakly compressible approximation, k_0 is chosen so that the Mach number is about M=0.1)

$$p_1 = k_0 \left(\left(\frac{\rho_1}{\rho_0} \right)^{\gamma} - 1 \right)$$

The pressure does not depend on energy, so the energy equations can be dropped.

The interface velocity is supposed to be the one of the liquid phase.

$$\vec{v}_I = \vec{v}_1$$

The interface pressure is supposed to be the one of the gas phase.

$$p_I = p_2 = p_0 = 0$$

Special Case of the Baer-Nunziato Model

$$\frac{\partial}{\partial t}(\alpha_1\rho_1) + \nabla\cdot(\alpha_1\rho_1\vec{v}_1) = 0,$$

$$\frac{\partial}{\partial t}(\alpha_1\rho_1\vec{v}_1) + \nabla\cdot(\alpha_1(\rho_1\vec{v}_1\vec{v}_1 + p_1)) - \cancel{p_I\nabla\alpha_1} = 0,$$

$$\cancel{\frac{\partial}{\partial t}(\alpha_1\rho_1 E_1) + \nabla\cdot(\alpha_1\vec{v}_1(\rho_1 E_1 + p_1)) + p_I\frac{\partial}{\partial t}\alpha_1 = 0,}$$

$$\xcancel{\frac{\partial}{\partial t}(\alpha_2\rho_2) + \nabla\cdot(\alpha_2\rho_2\vec{v}_2) = 0,}$$

$$\xcancel{\frac{\partial}{\partial t}(\alpha_2\rho_2\vec{v}_2) + \nabla\cdot(\alpha_2(\rho_2\vec{v}_2\vec{v}_2 + p_2)) - p_I\nabla\alpha_2 = 0,}$$

$$\xcancel{\frac{\partial}{\partial t}(\alpha_2\rho_2 E_2) + \nabla\cdot(\alpha_2\vec{v}_2(\rho_2 E_2 + p_2)) + p_I\frac{\partial}{\partial t}\alpha_2 = 0,}$$

$$\frac{\partial}{\partial t}\alpha_1 + \vec{v}_I\cdot\nabla\alpha_1 = 0,$$

Special Case of the Baer-Nunziato Model

These assumptions yield the following simplified three-equation model:

$$
\begin{aligned}
&\frac{\partial}{\partial t}(\alpha\rho) + \nabla\cdot(\alpha\rho\vec{v}) = 0,\\
&\frac{\partial}{\partial t}(\alpha\rho\vec{v}) + \nabla\cdot(\alpha(\rho\vec{v}\vec{v} + p\mathbf{I})) = \alpha\rho\vec{g},\\
&\frac{\partial}{\partial t}\alpha + \vec{v}\cdot\nabla\alpha = 0,
\end{aligned}
\qquad \text{(SBN)}
$$

(SBN) can be interpreted as a weakly compressible formulation of the volume-of fluid (VOF) method [Hirt & Nichols].

2D Test Problems

Overtopping flow over a sharp-crested weir

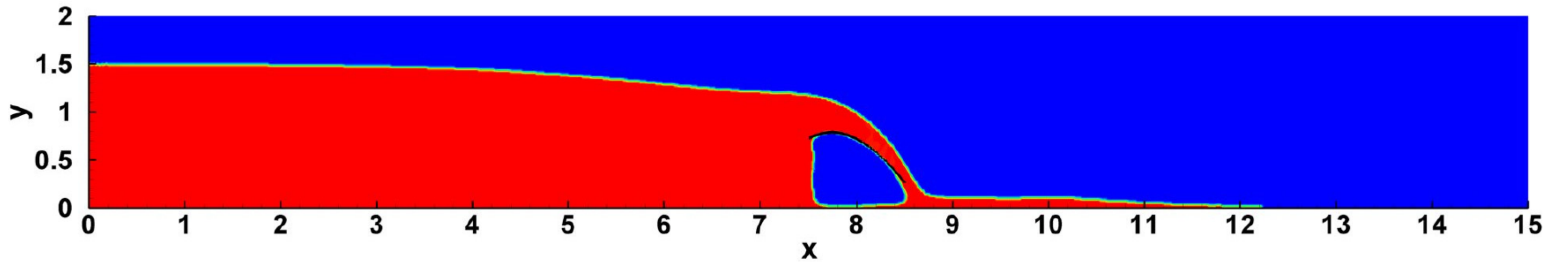

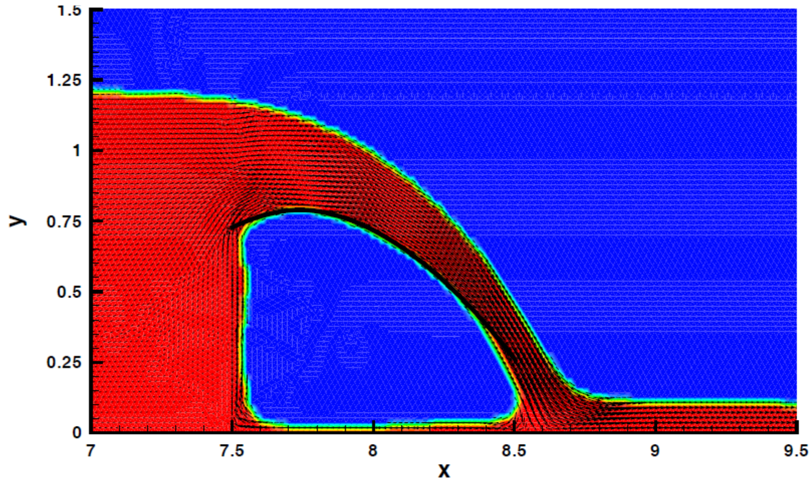

Density contour lines. The thick solid line indicates the experimental reference solution of [Scimemi, 1930].

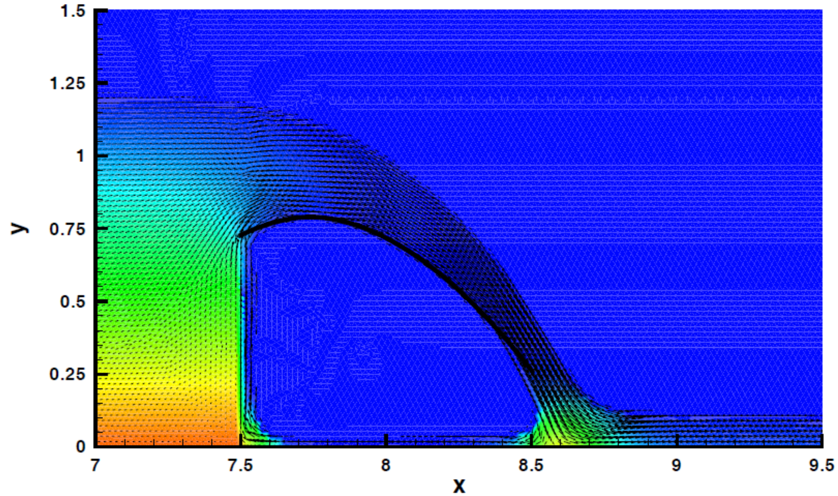

Pressure contours. Note the pressure distribution in the reservoir, in the free jet and at the stagnation point.

3D Test Problems

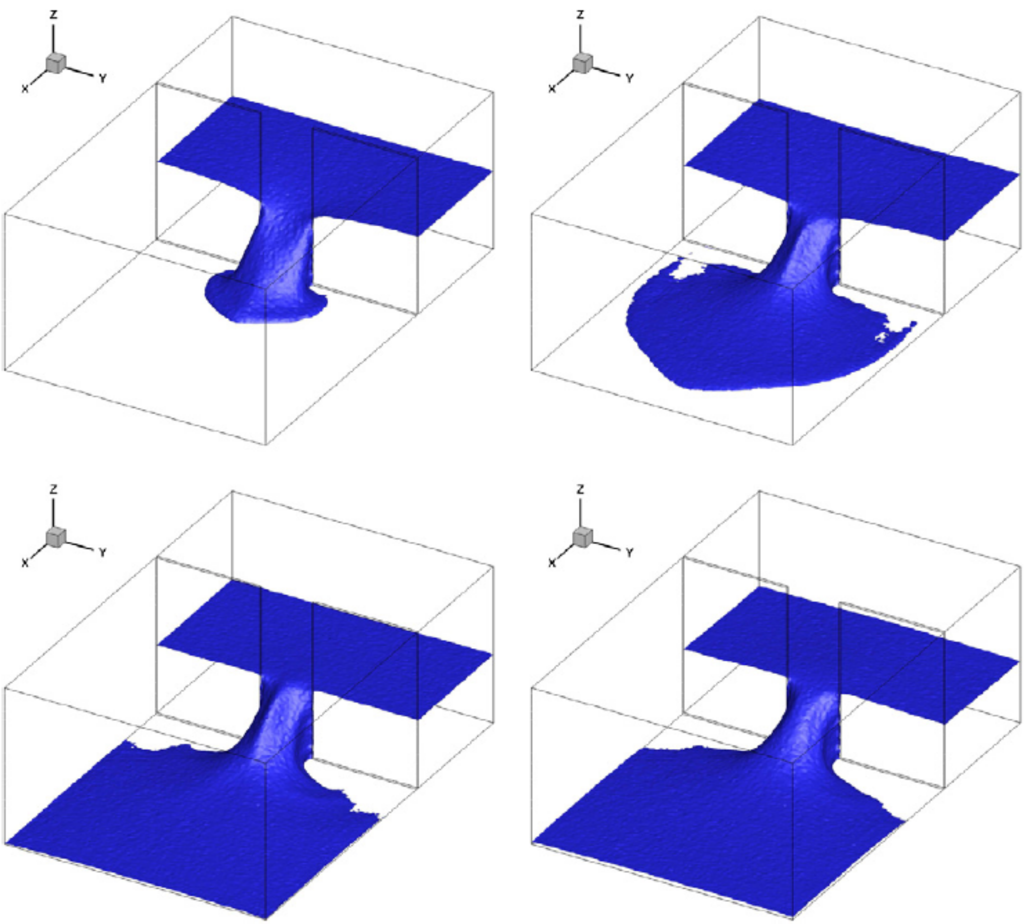

3D Dambreak problem [Fraccarollo & Toro 1995]

3D Test Problems

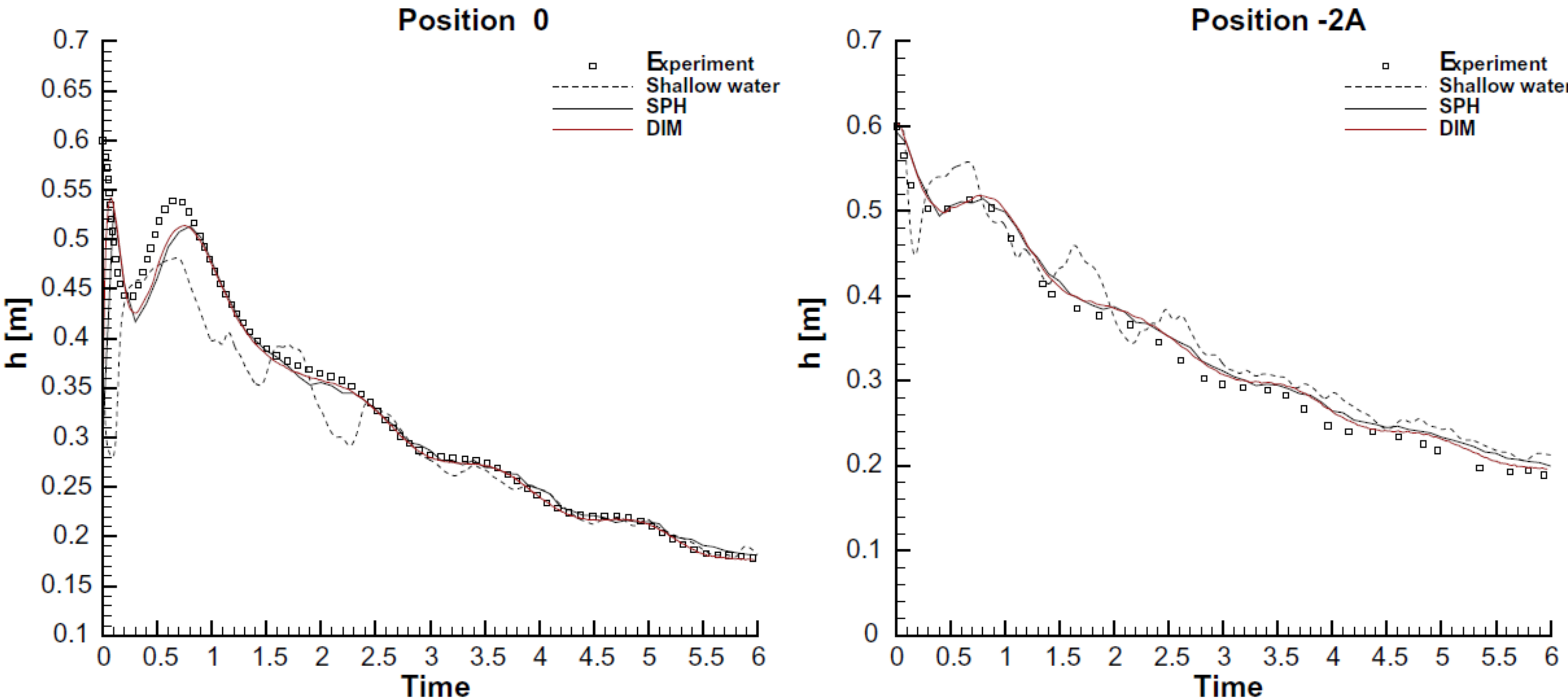

3D Dambreak problem [Fraccarollo & Toro 1995]

3D Test Problems

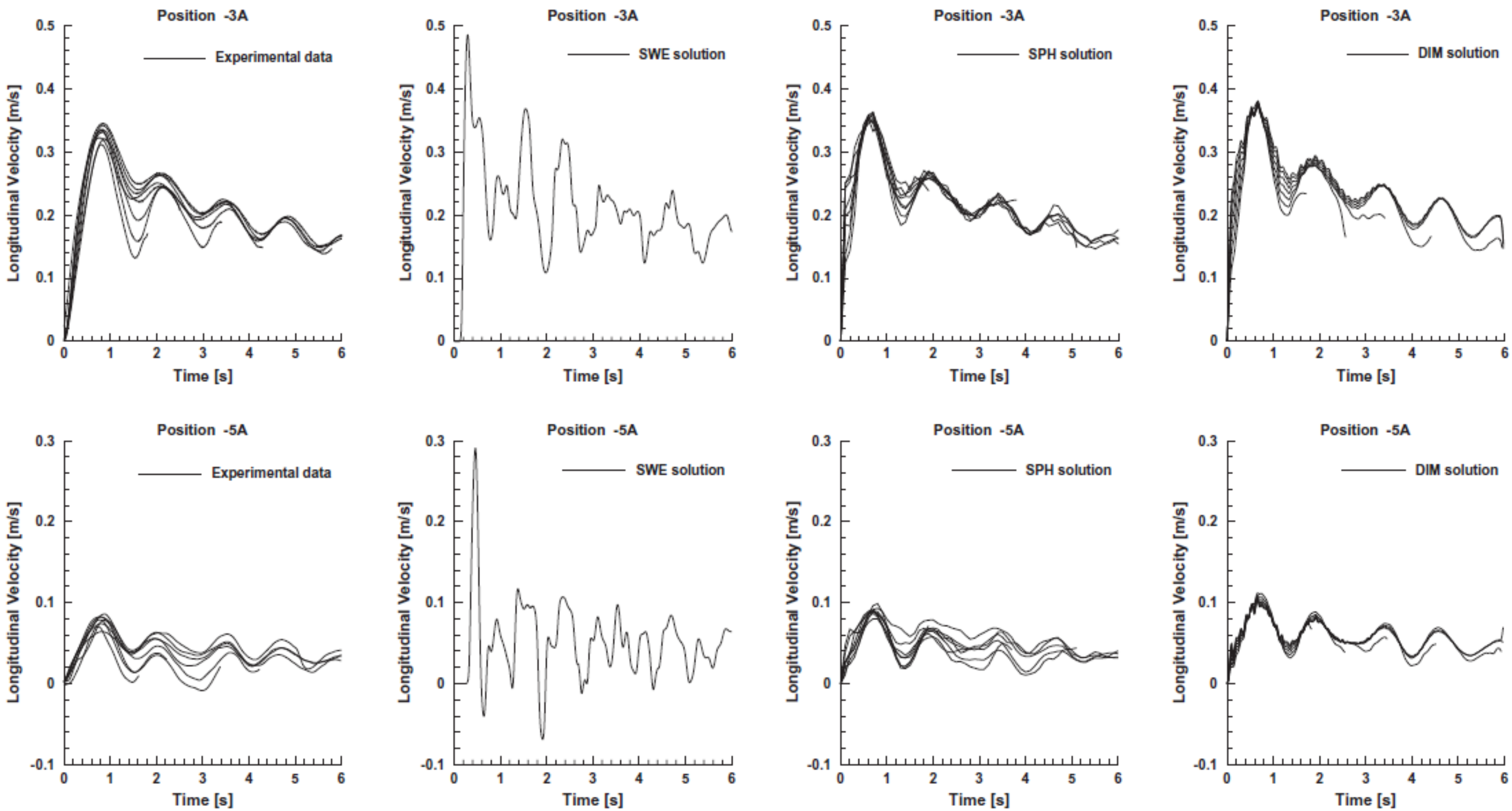

3D Dambreak problem [Fraccarollo & Toro 1995]

3D Test Problems

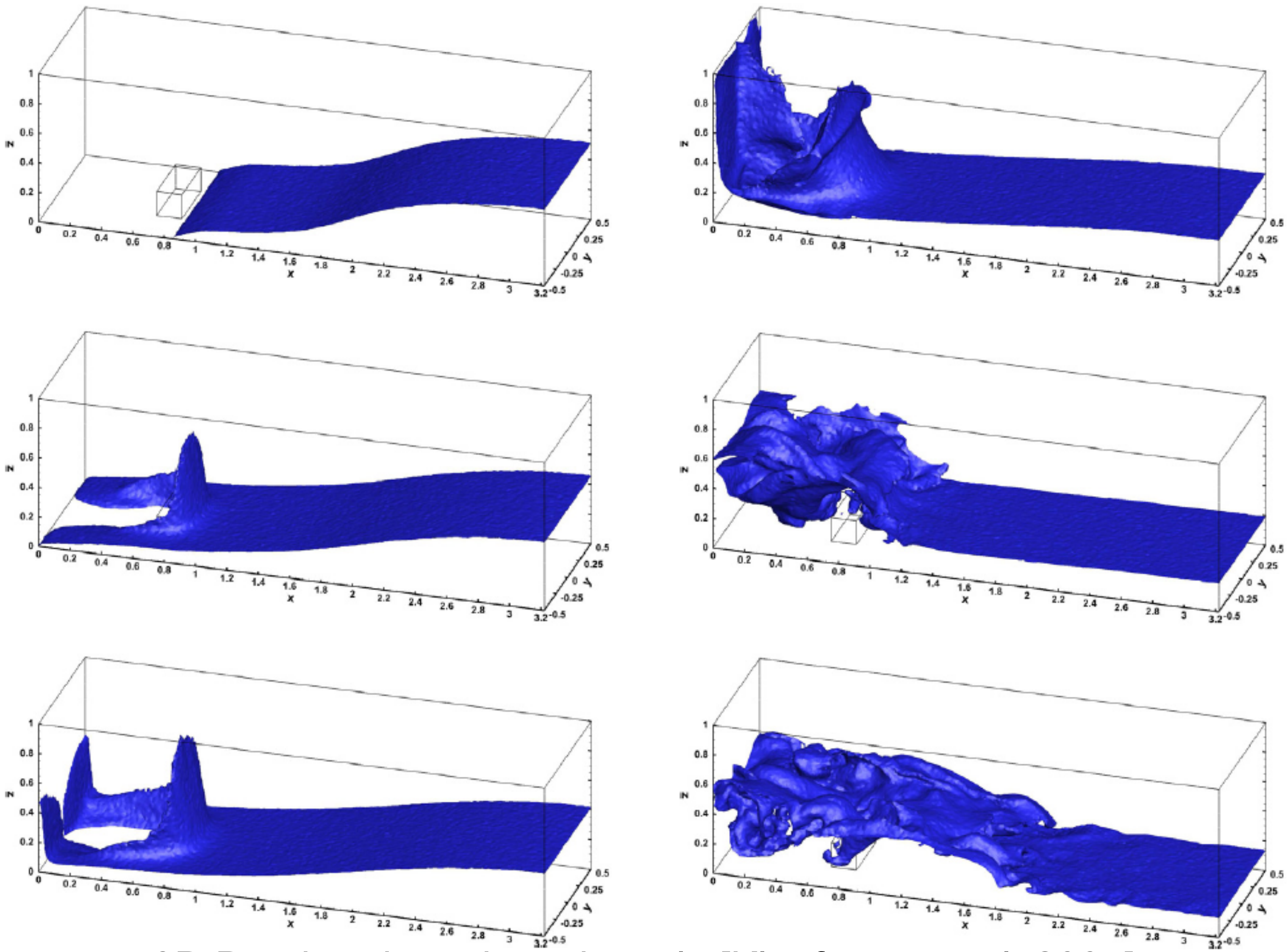

3D Dambreak against obstacle [Kleefsman et al. 2005]

3D Test Problems

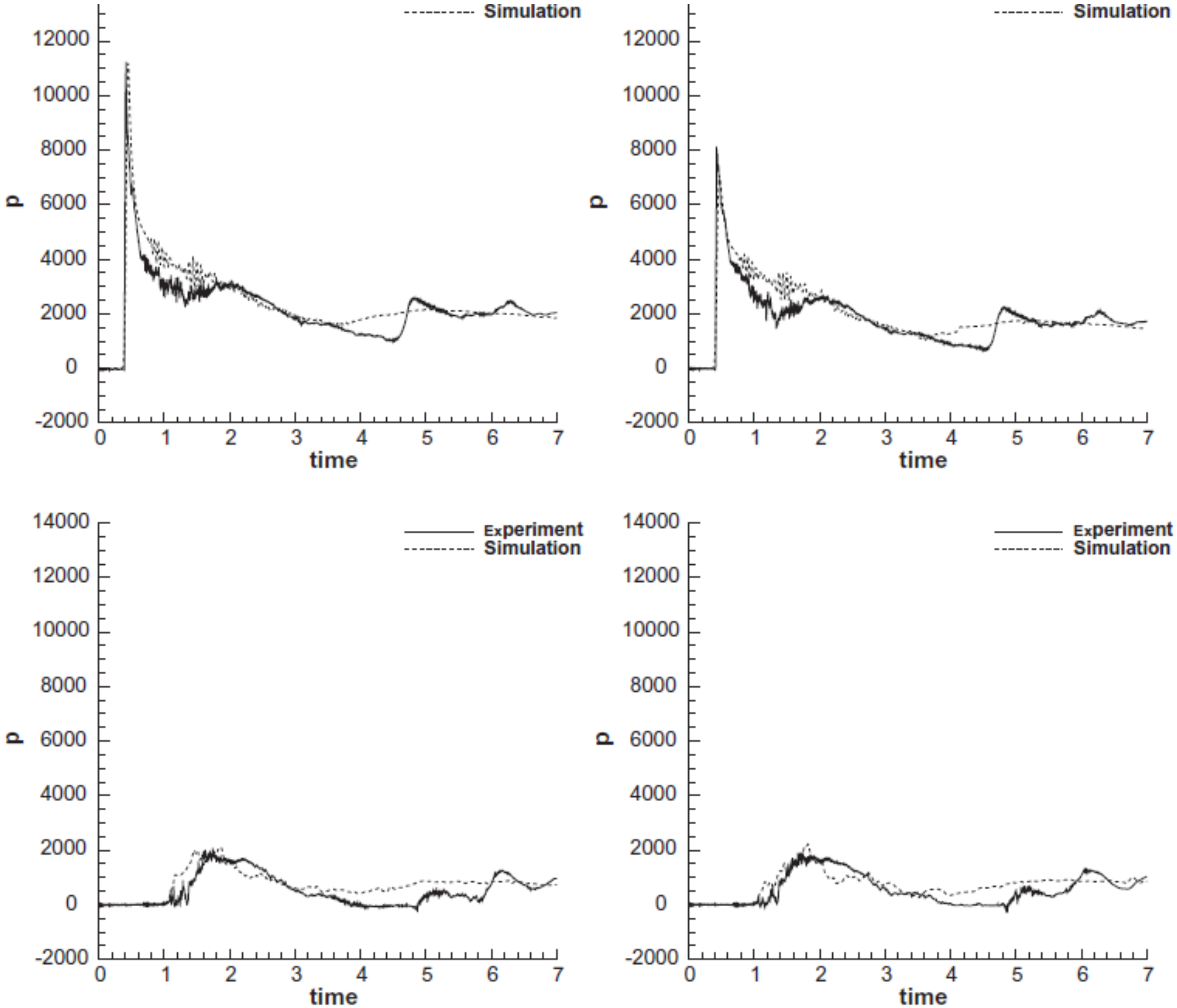

3D Dambreak against obstacle [Kleefsman et al. 2005]

List of References

[1] M. Dumbser, M. Käser, V. Titarev, E.F. Toro. **Quadrature-Free Non-Oscillatory Finite Volume Schemes on Unstructured Meshes for Nonlinear Hyperbolic Systems,** *Journal of Computational Physics, vol.* ***226****:204-243, 2007.*

[2] M. Dumbser, D.S. Balsara, E.F. Toro and C.D. Munz. **A Unified Framework for the Construction of One-Step Finite-Volume and Discontinuous Galerkin Schemes on Unstructured Meshes**, *Journal of Computational Physics*, 227(18):8209–8253, 2008.

[3] M. Dumbser, C. Enaux and E. F. Toro. **Finite Volume Schemes of Very High Order of Accuracy for Stiff Hyperbolic Balance Laws**, *Journal of Computational Physics,* 227(8):3971–4001, 2008

[4] M. Dumbser. **Arbitrary High Order $P_N P_M$ Schemes on Unstructured Meshes for the Compressible Navier-Stokes Equations**, *Computers & Fluids*, 39(1):60-76, 2010.

[5] M. Dumbser and O. Zanotti. **Very High Order $P_N P_M$ Schemes on Unstructured Meshes for the Resistive Relativistic MHD Equations**. *Journal of Computational Physics,* 228(18):6991–7006, 2009.

[6] M. Dumbser, M. Castro, C. Parés and E.F. Toro. **ADER schemes on Unstructured Meshes for Nonconservative Hyperbolic Systems: Applications to Geophysical Flows.** *Computers & Fluids,* 38(9):1731-1748, 2009

[7] M. Dumbser, A. Hidalgo, M. Castro, C. Parés and E.F. Toro. **FORCE Schemes on Unstructured Meshes II: Non-Conservative Hyperbolic Systems.** *Computer Methods in Applied Mechanics and Engineering*, 199(9-12):625-647, 2010

[8] M. Dumbser and E.F. Toro. **A Simple Extension of the Osher Riemann Solver to Non-Conservative Hyperbolic Systems**. *Journal of Scientific Computing*, 48:70-88, 2011

[9] M. Dumbser and E.F. Toro. **On Universal Osher-Type Schemes for General Nonlinear Hyperbolic Conservation Laws**. *Communications in Computational Physics*, 10(3): 635-671,2011

[10] M. Dumbser. **A Diffuse Interface Method for Complex Three-Dimensional Free Surface Flows**. *Computer Methods in Applied Mechanics and Engineering,* 257:47-64, 2013

[11] M. Dumbser, O. Zanotti, A. Hidalgo and D.S. Balsara. **ADER-WENO Finite Volume Schemes with Space-Time Adaptive Mesh Refinement**, *Journal of Computational Physics,* 248:257-286, 2013

[12] M. Dumbser and W. Boscheri. **High-Order Unstructured Lagrangian One-Step WENO Finite Volume Schemes for Non-Conservative Hyperbolic Systems: Applications to Compressible Multi-Phase Flows**. *Computers and Fluids,* 86:405-432, 2013